

Tectonostratigraphic evolution of the Slyne Basin

Conor M. O'Sullivan^{1,2,4}, Conrad J. Childs^{1,2}, Muhammad M. Saqab^{1,2,5}, John J. Walsh^{1,2}, Patrick M. Shannon^{1,3}

¹ Irish Centre for Research in Applied Geoscience (iCRAG), O'Brien Centre for Science (East), University College Dublin, Belfield, Dublin 4, Ireland

² Fault Analysis Group, School of Earth Sciences, University College Dublin, Belfield, Dublin 4, Ireland

³ School of Earth Sciences, University College Dublin, Belfield, Dublin 4, Ireland

⁴ Present address: Petroleum Experts, Petex House, 10 Logie Mill, Edinburgh, EH7 4HG, United Kingdom

⁵ Present address: Norwegian Geotechnical Institute, 40 St. Georges Terrace, Perth, WA 6000, Australia

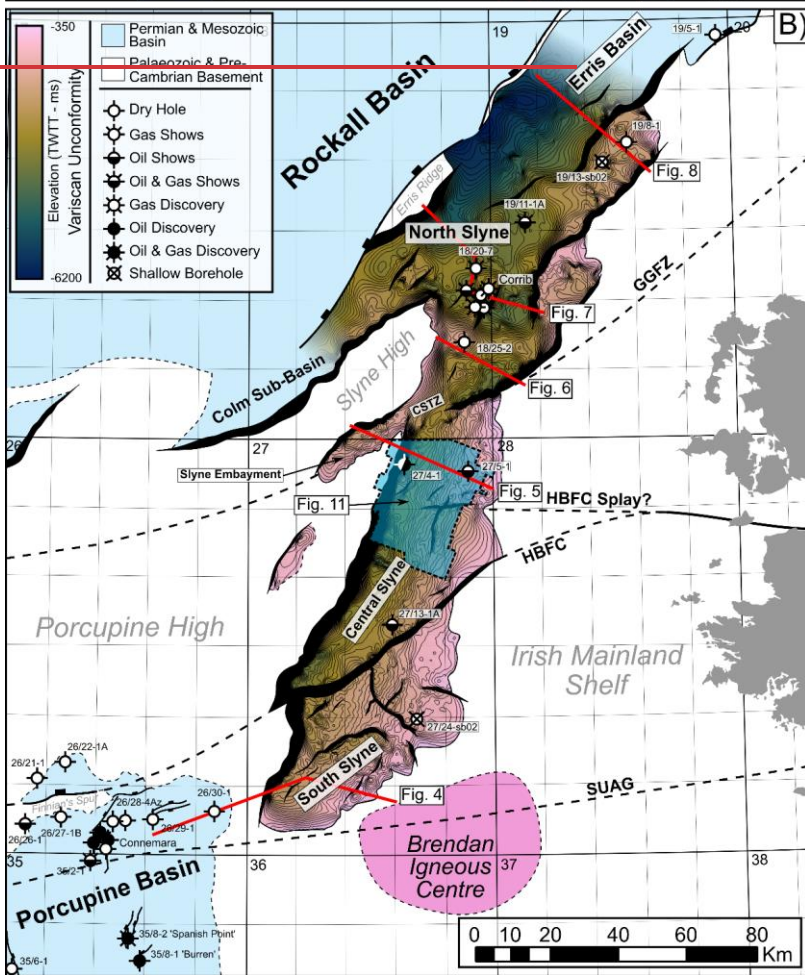
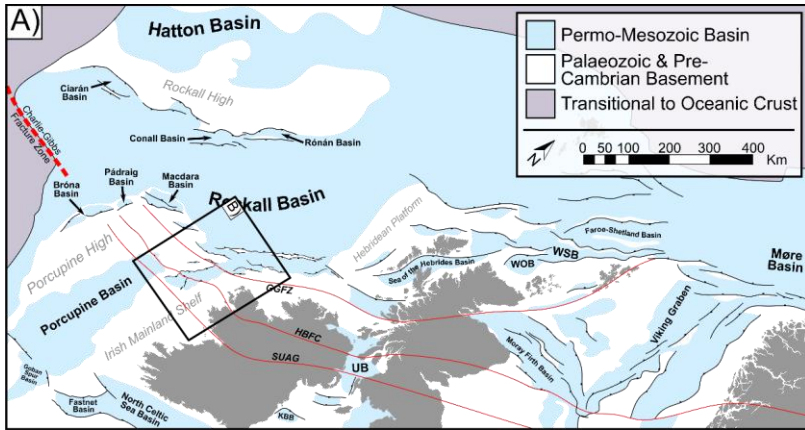
Corresponding author email: cmnosullivan@gmail.com

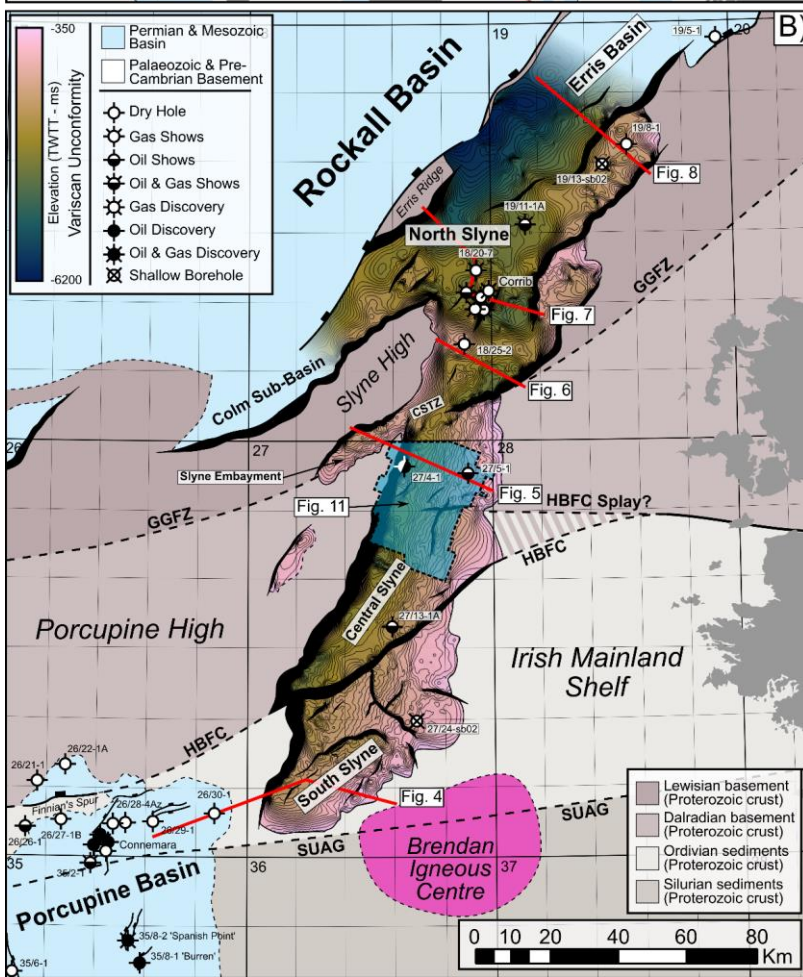
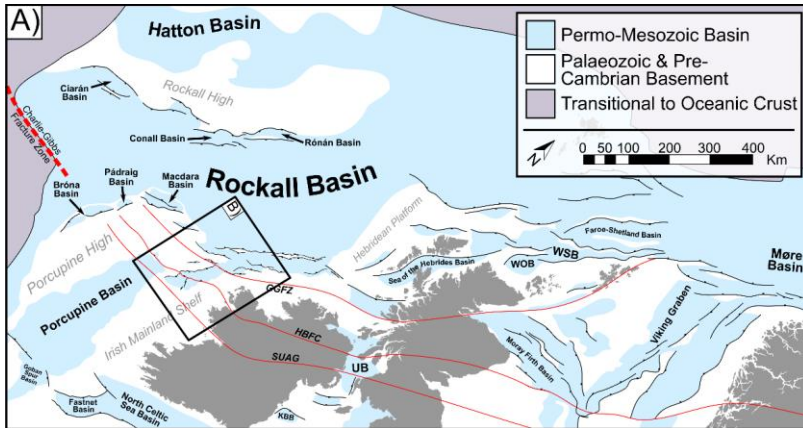
1. Abstract

The Slyne Basin, located offshore NW Ireland, is a narrow and elongate basin composed of a series of interconnected grabens and half-grabens, separated by transfer zones coincident with deep ~~Caledonian-aged~~ crustal structures formed during the Silurian to Devonian aged Caledonian Orogeny. The basin is the product of a complex, polyphase structural evolution stretching from the Permian to the Miocene. ~~Relatively~~Initially, relatively low-strain ~~episodic~~ rifting occurred in the Late Permian and again in the latest Triassic to Middle Jurassic, ~~with the main~~followed by a third phase of high-strain rifting ~~occurring in~~during the Late Jurassic. These extensional events were punctuated by periods of tectonic quiescence during the Early Triassic, and ~~regional uplift and erosion during the late~~ Middle Jurassic. Late Jurassic strain was primarily accommodated by several kilometres of slip on the basin-bounding faults, which formed through the breaching of relay ramps between left-stepping fault segments developed during earlier Permian and Early-Mid Jurassic rift phases. Following the cessation of rifting at the end of the Jurassic, the area experienced kilometre-scale uplift and erosion during the Early Cretaceous and second, less-severe phase of denudation during the Palaeocene. These post-rift events formed ~~a~~ distinct regional post-rift ~~unconformity~~unconformities and resulted in a reduced post-rift sedimentary section. The structural evolution of the Slyne Basin ~~is~~was influenced by pre-existing Caledonian structures at a high angle to the basinal trend. The basin illustrates a rarely documented style of fault reactivation in which basin-bounding faults are oblique to the earlier structural trend, but the initial fault segments are parallel to this trend. The result is a reversal of the sense of stepping of the initial fault segments generally associated with basement control on basin-bounding faults.

34 2. Introduction

35 The north-western European Atlantic margin is made up of a framework of basins which are
36 the product of a polyphase geological evolution stretching from Variscan orogenic collapse at
37 the end of the Carboniferous to the formation of oceanic crust in the Eocene during the opening
38 of the North Atlantic Ocean (Fig. 1A). The evolution of these basins is influenced by a variety
39 of factors, including pre-existing faults and lineaments, typically inherited from the Caledonian
40 or Variscan orogenies, and the presence of salt within the sedimentary basin-fill, acting as
41 layers of mechanical detachment. Pre-existing Caledonian and Variscan structures have been
42 observed both reactivating and influencing the formation of younger structures during later Late
43 Paleozoic and Mesozoic rift events if oriented optimally (e.g. Stein, 1988; Schumacher, 2002;
44 Wilson et al., 2010; Bird et al., 2014; Fazlikhani et al., 2017; Osagiede et al., 2020) or acting
45 as barriers to fault growth and segmenting rift systems if they are oblique to the extension
46 direction (e.g. Morley et al., 2004; Pereira et al., 2011; Pereira & Alves, 2013; Philips et al.,
47 2018).





50 **Figure 1: A)** Simplified structural map of the NW European Atlantic margin showing the study
51 area in relation to other Permian & Mesozoic sedimentary basins, adapted from Doré et al.,
52 1999 and Naylor et al., 1999. Caledonian structural lineaments which segment the basins are
53 lighted in red. **Abbreviations:** GGFZ, Great Glen Fault Zone; HBFC, Highland Boundary- Fair
54 Head–Clew Bay Lineament; KBB, Kish Bank Basin; SUAG, Southern Uplands- Antrim-
55 Galway Lineament; UB, Ulster Basin; WOB, West Orkney Basin; WSB, West Shetland Basin..
56 **B)** Time structure map of the Base Permian or Variscan Unconformity in the Slyne Basin.
57 Local sub-basins and structural elements are labelled. Approximate location of Caledonian
58 structures are highlighted outside the Slyne Basin with dashed black lines. Primary basement
59 composition adapted from Štolfová & Shannon, 2009. **Abbreviations:** CSTZ – Central Slyne
60 Transfer Zone.

61 The Slyne Basin (250 km long and between 30 and 70 km wide) is a ~~narrow~~ chain of grabens
62 and half-grabens that occupy the eastern margin of the Rockall Basin (Fig. 1). The Slyne Basin
63 shows significant along-strike structural variability, with changes in dip direction of the
64 kilometre-scale basin-bounding faults occurring over relatively short distances i.e. at transfer
65 zones. The transfer zones have been interpreted as areas commonly observed where
66 crustal-scale lineaments and terrane boundaries of Caledonian age transect the younger Late
67 Palaeozoic and Mesozoic rifts. Similar phenomena have been observed in rift basins across
68 the world, where pre-existing zones of weakness can be reactivated if oriented
69 optimally influence the development of younger structures and where strain is transferred
70 between them i.e. the formation of transfer zones between large fault systems. The north-
71 western European Atlantic margin is underlain by a series of pre-existing structures and
72 structural inheritance ~~and reactivation~~ has been well documented in the Norwegian and UK
73 Atlantic margins (Doré et al., 1999; Doré et al., 2007; Ady & Whittaker, 2019; Schiffer et al.,
74 2019) as well as in the Iberian Atlantic margin (Alves et al., 2006; Pereira et al., 2017).

75 The structural geology of the Slyne Basin was the subject of significant study during the late
76 1990s and early 2000s following the discovery of the Corrib gas field in 1996 (Dancer et al.,
77 2005). Previous publications documented aspects of the structural evolution (Chapman et al.,
78 1999; Dancer et al., 1999) and the role of exhumation in the petroleum system of the basin
79 (Corcoran & Doré, 2002; Corcoran & Mecklenburgh, 2005), as well placing the basin in the
80 regional context of the Irish Atlantic margin (e.g. Corfield et al., 1999; Walsh et al., 1999). In
81 recent years, significantly more and higher quality seismic data, together with additional well
82 data have been acquired throughout the Slyne Basin and neighbouring areas (Shannon,
83 2018). Additionally, a comprehensive biostratigraphic study of all the Irish offshore basins has
84 reclassified the ages of key syn-rift sequences (Merlin Energy Resources Consortium, 2020),
85 warranting fresh investigation into the structural evolution of the Slyne Basin and its context
86 within the greater Irish Atlantic margin.

87 This study utilizes an extensive database of borehole-constrained 2D and 3D seismic
88 reflection data, coupled with the results from the new biostratigraphic database, to investigate

89 the structural evolution of the Slyne Basin. Key aspects of this structural history, including the
90 development of the major basin-bounding faults, the role of salt in basin evolution, and
91 influence of pre-existing crustal-structures in the segmentation of the Slyne basin are
92 examined and characterised. These findings are then placed in a regional context to better
93 understand the role of the Slyne Basin in the evolution of the greater Irish Atlantic margin.

94 3. Geological Setting

95 The Slyne Basin has a relatively flat present-day bathymetry, with water depths ranging from
96 100 to 600m across most of the study area, with water depths increasing up to 2500m in the
97 north (Dancer et al., 1999). It is divided into three distinct sub-basins: the Northern, Central
98 and Southern Slyne sub-basins (Fig. 4.1B, sensu Trueblood & Morton, 1991). These are
99 separated by transfer zones (e.g. sensu Morley et al., 1990; Gawthorpe & Hurst, 1993) which
100 coincide with the location of major structural lineaments, in the form of Caledonian terrane
101 boundaries. Three Caledonian structures are mapped in Figure 1B.

102 The Slyne Basin is bounded along its eastern margin by the Irish Mainland Shelf, while the
103 Porcupine and Slyne highs make up the western boundary (Fig. 1B). The Colm Basin,
104 previously identified as a distinct Mesozoic basin (Dancer et al., 1999), appears to be an
105 extension of the Northern Slyne Sub-basin, verging south-westwards between the Rockall
106 Basin and the Porcupine High. A narrow, discontinuous basement horst which represents a
107 southern extension of the Erris Ridge (Cunningham & Shannon, 1997) separates the Northern
108 Slyne Sub-basin and the neighbouring Erris Basin from the Rockall Basin to the northwest.
109 Similarly, a narrow basement high separates the Southern Slyne Sub-basin from the
110 Porcupine Basin to the southwest.

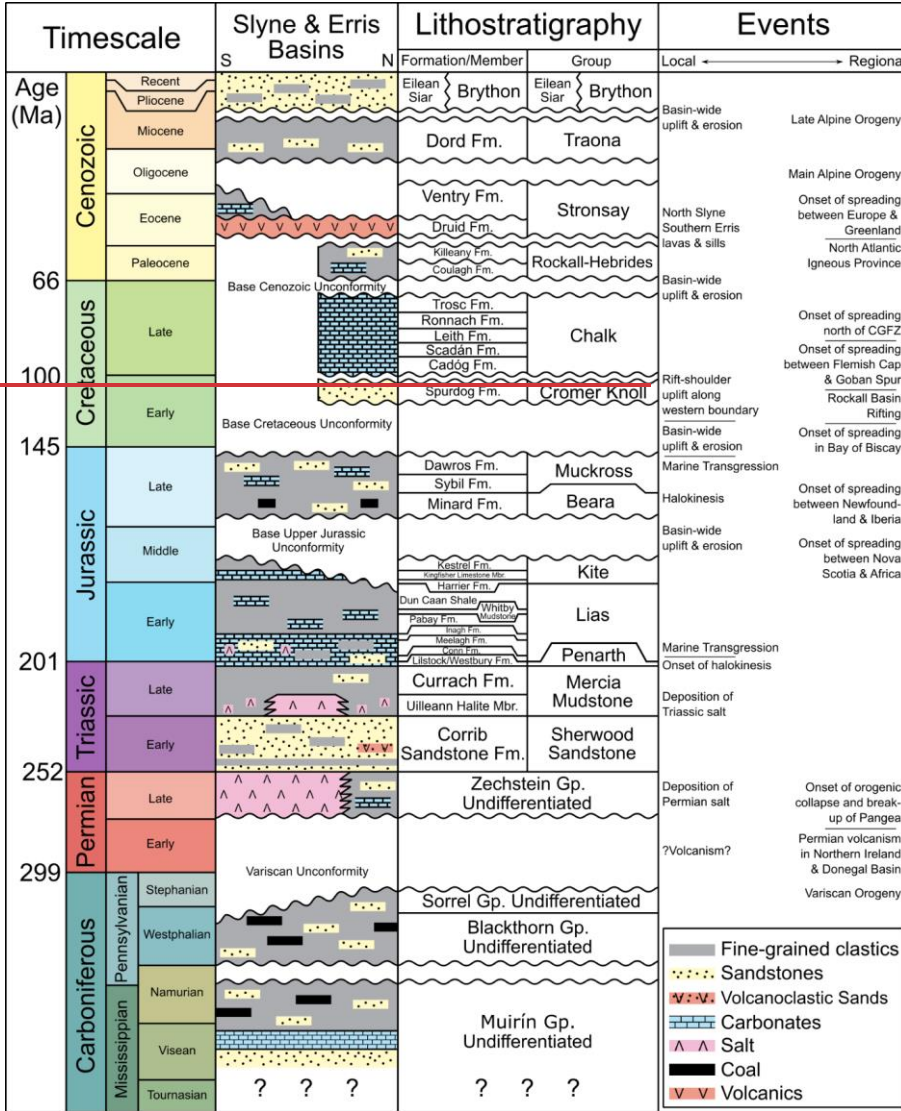
111 3.1. Basement configuration

112 Previous authors have noted the role of pre-existing Caledonian structures in the
113 segmentation of younger Mesozoic basins on the Irish Atlantic margin, correlating the offshore
114 extension of these crustal-scale structures with complex transfer zones separating distinct
115 sub-basins (Trueblood & Morton, 1991; Dancer et al., 1999). Several authors have mapped
116 the offshore extent of Caledonian structural lineaments on the Irish Atlantic margin (Lefort &
117 Max, 1984; Tate, 1992; Naylor & Shannon, 2005; Štolfova & Shannon, 2009; Kimbell et al.,
118 2010). There are three Caledonian structures relevant to the evolution of the Slyne Basin; the
119 Great Glen Fault Zone (GGFZ), the Highland Boundary-Fair Head Clew Bay Fault Zone
120 (HBFC) and the Southern Uplands-Antrim Galway Fault Zone (SUAG, Fig. 1B). The exact
121 locations of these structures in the vicinity of the Slyne Basin are variably constrained; the NE-
122 SW trending GGFZ has been mapped across the Irish Mainland Shelf to the west of the Erris

123 Basin using deep seismic profiles and potential field datasets as a vertical strike-slip fault
124 (Klemperer et al., 1991; Kimbell et al., 2010). The GGFZ intersects the Slyne Basin between
125 the Northern and Central Slyne sub-basins at a location termed the Central Slyne Transfer
126 Zone (CSTZ, sensu Dancer et al., 1999). The HBFC and SUAG structures are more poorly
127 constrained; the HBFC is an E-W oriented structure bounding the southern shore of Clew Bay
128 on the west coast of Ireland and is mapped passing through Clare Island due west of Clew
129 Bay (Fig. 1, Badley, 2001; Worthington & Walsh, 2011). The HBFC may correlate with the
130 fault zone separating the Central and Southern Slyne sub-basins, but there is also evidence
131 that splays of the HBFC may also be observed in the Central Slyne Sub-basin (Fig. 1B). The
132 SUAG structure has been mapped trending E-W along the northern shore of Galway Bay
133 (REF) and south of the Slyne Basin, through the Brendan Igneous Centre (Fig. 1).
134 These Unlike the GGFZ, both the HBFC and SUAG structures are more shallowly dipping
135 normal and reverse fault zones, although evidence of strike-slip movement is recorded along-
136 strike onshore Ireland (Badley, 2001; Worthington & Walsh, 2011; Anderson et al., 2018).
137 The Caledonian lineaments separate different basement terranes which were assembled
138 during the Caledonian Orogeny and have been extended from their known extents onshore
139 Ireland and Scotland by several authors (e.g. Roberts et al., 1999; Tyrrell et al., 2007; Štolfová
140 & Shannon, 2009). Limited pre-Carboniferous well penetrations in the Slyne Basin preclude
141 the accurate mapping of these basement terranes and the interpretations of previous authors
142 are adopted here.

143 3.2. Stratigraphic framework of the Slyne Basin

144 Previous stratigraphic nomenclature for the Slyne Basin was largely based on comparisons
145 with the geology of the Hebridean basins exposed on the Isle of Skye (e.g. Trueblood &
146 Morton; 1991). An updated stratigraphic nomenclature with revised biostratigraphy has
147 recently been published, standardising nomenclature at group, formation and member levels
148 across the sedimentary basins of the Irish Continental Shelf (Merlin Energy Resources
149 Consortium, 2020). This stratigraphic nomenclature is used in this study (Fig. 2). The
150 main high-strain Middle Jurassic syn-rift section of previous authors (e.g. Chapman et al.,
151 1999; Dancer et al., 1999; Corcoran & Mecklenburgh, 2005; Dancer et al., 2005) has recently
152 been reclassified as Late Jurassic in age. This has important implications for regional
153 geodynamics which are discussed below. For full details on the biostratigraphic
154 reclassification please refer to Merlin Energy Resources Consortium (2020).

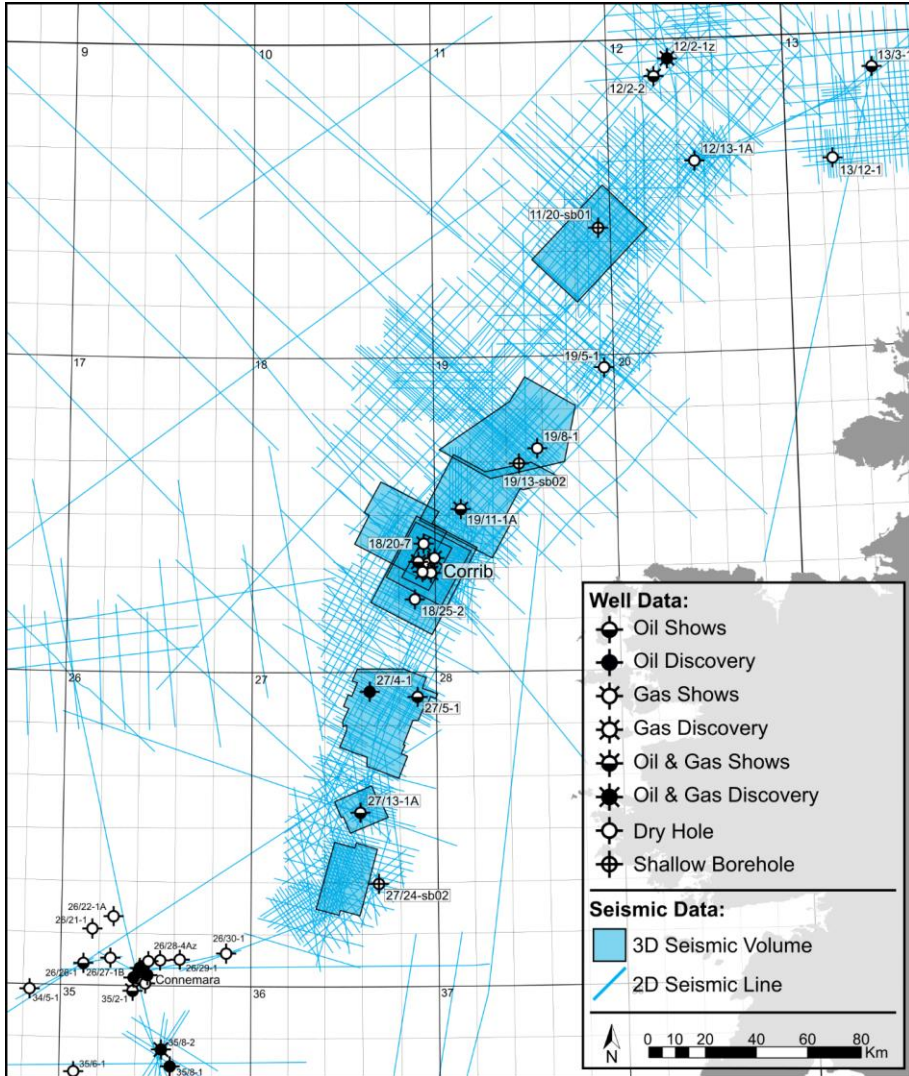


170 The Lower Jurassic section is composed of marine sandstone, mudstones and carbonates,
171 overlain by Middle Jurassic calcareous marine mudstones (Trueblood & Morton, 1991; Dancer
172 et al., 1999). The Kingfisher Limestone Member is a unit of thick limestones that occurs at the
173 base of Kestrel Formation (sensu Merlin Energy Resources Consortium, 2020) and which
174 forms a distinct, semi-regional seismic marker termed the 'Bajocian Limestone Marker' in
175 previous literature (e.g. Trueblood & Morton, 1991; Scotchman & Thomas, 1995; Dancer et
176 al., 1999). A regional unconformity separates the underlying Lower and Middle Jurassic
177 sections from the overlying Upper Jurassic sediments. The Upper Jurassic section consists of
178 terrestrial and fluvio-estuarine mudstones and sandstones with numerous palaeosols and coal
179 layers, which are overlain by the marine mudstones, indicating a regional marine transgression
180 occurred during the late Oxfordian to Tithonian (Merlin Energy Resources Consortium, 2020).

181 The Base-Cretaceous Unconformity separates the Cretaceous section of the Slyne Basin from
182 the underlying Jurassic strata. The Lower Cretaceous stratigraphy consists of Albian-aged
183 glauconitic mudstones and sandstones, while the overlying Upper Cretaceous section is
184 composed of limestones and calcareous mudstones. The Base-Cenozoic Unconformity forms
185 the lower boundary to the Cenozoic succession in the Slyne Basin. The Cenozoic section can
186 be subdivided into three sequences: a layer of Eocene lava locally developed in the northern
187 and southern areas of the Slyne Basin, overlain by an Eocene-Miocene section and a Miocene
188 to Quaternary section, both consisting of poorly consolidated marine mudstones and
189 sandstones, separated by a mid-Miocene unconformity.

190 4. Dataset &and Methodology

191 This study focused on the interpretation of an extensive suite of multi-vintage 2D and 3D
192 seismic reflection data collected during hydrocarbon exploration in the Slyne Basin (Fig. 3).
193 The 2D seismic dataset consists of 17 surveys acquired between 1980 and 2007, comprising
194 over 22,000 line-kilometres of data, while the 3D seismic dataset consists of eight surveys
195 acquired between 1997 and 2013 and covers almost 4,000 square-kilometres. Seismic data
196 quality varies from very poor to good, with the more modern vintages typically providing clearer
197 imaging. Data quality in the Slyne Basin is heavily influenced by the near-seabed geology,
198 with the distribution of Cenozoic lava flows and intrusive sills, coupled with Cretaceous chalk
199 causing imaging problems including multiples, energy scattering and signal attenuation
200 (Dancer & Pillar, 2001). These problems are most severe in the Northern Slyne Sub-basin,
201 and the western margin of the Southern Slyne Sub-basin. The application of modern
202 processing techniques and use of 3D seismic data has improved data quality in the region
203 somewhat (Dancer & Pillar, 2001; Droujinine et al., 2005; Rohrman, 2007; Hardy et al., 2010),
204 most recently with the acquisition of an ocean-bottom cable survey over the Corrib gas field
205 in 2012 and 2013 (Shannon, 2018). Seismic sections are presented in European polarity
206 (Brown, 2001), where a positive downwards increase in acoustic impedance corresponds to
207 a positive (red) reflection event and a decrease corresponds to a negative (blue) reflection
208 event. All sections are vertically exaggerated by a factor of three and ball-ends are used to
209 highlight where a fault terminates within a certain stratigraphic package, while faults without
210 ball-ends are truncated by a younger unconformity.



211

212 **Figure 3:** Map showing study area and data sets used.

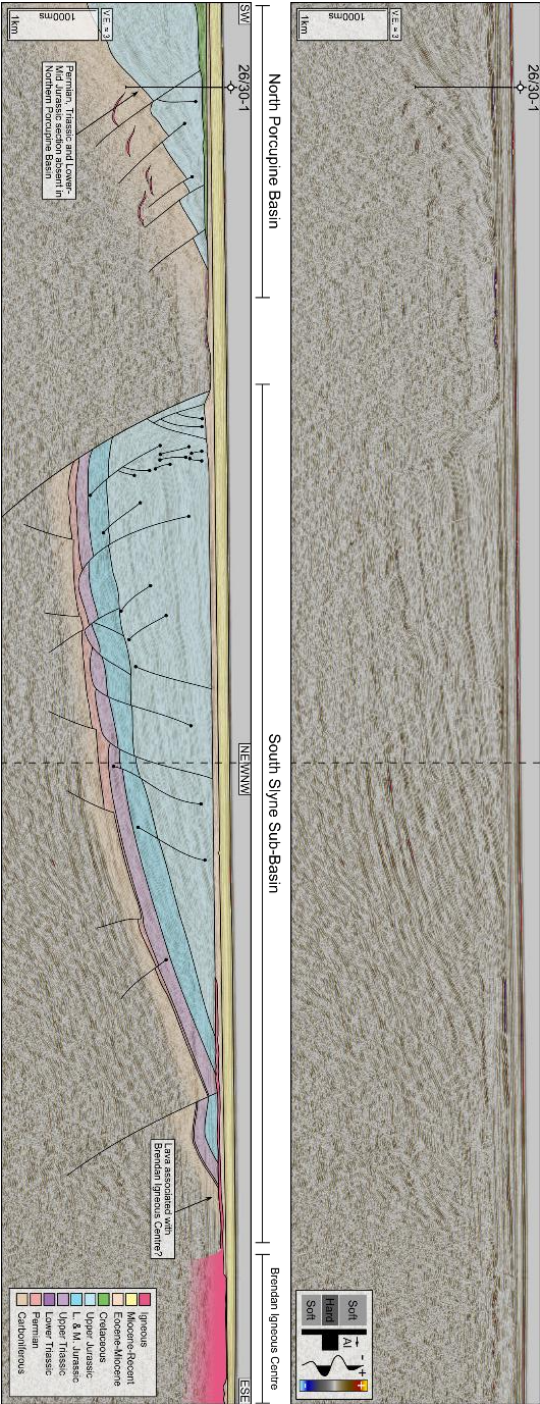
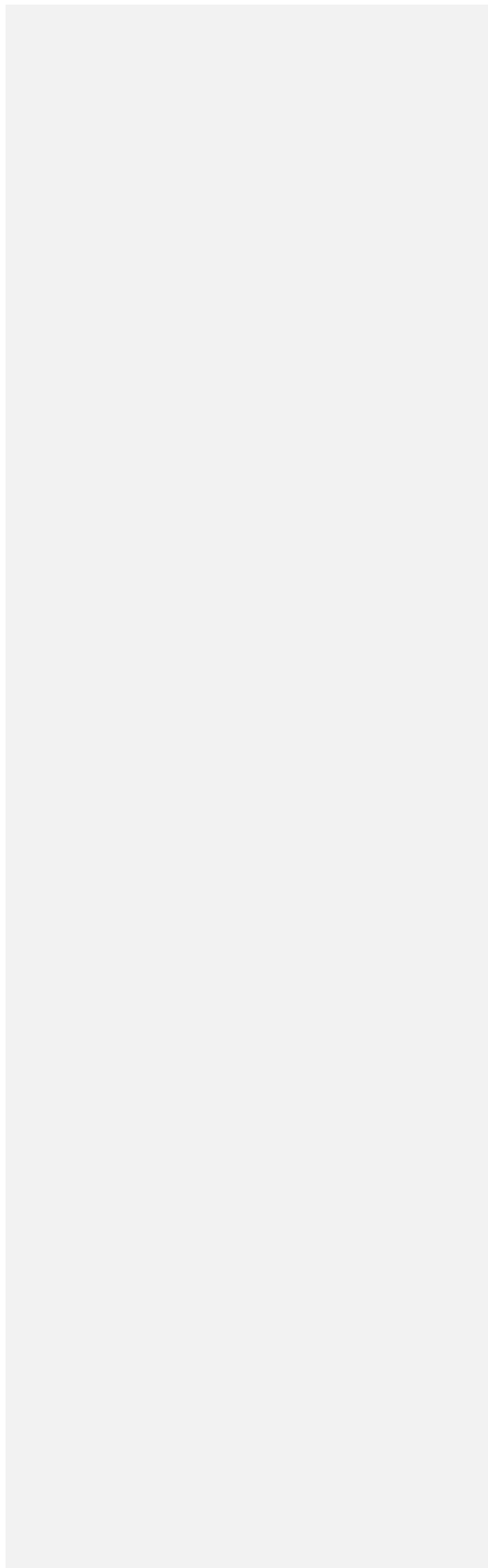
213 Thirteen key horizons were mapped across the Slyne Basin in the time domain (Fig. 2). The
 214 ages of these horizons were constrained using exploration and appraisal wells in addition to
 215 shallow boreholes. The Northern Slyne Sub-basin has the highest well density, including eight
 216 appraisal and production wells associated with the Corrib gas field, and four near-field
 217 exploration wells (19/8-1, 19/11-1A, 18/20-7 and 18/25-2), with a further three exploration
 218 wells in the Central Slyne Sub-basin (27/4-1, 27/5-1 and 27/13-1). The stratigraphy of the
 219 Southern Slyne Sub-basin is unconstrained except for a single shallow borehole (27/24-

220 sb02A) which proved Lower Jurassic and Upper Triassic sediments beneath the Base-
221 Cenozoic Unconformity (Fugro, 1994a). The dataset associated with the exploration, appraisal
222 and production wells consist of comprehensive suites of wireline logs (gamma, caliper,
223 neutron-density, sonic, and resistivity logs), well completion reports with formation tops, and
224 time-depth relationship data as either checkshots, or vertical seismic profiles (VSPs).

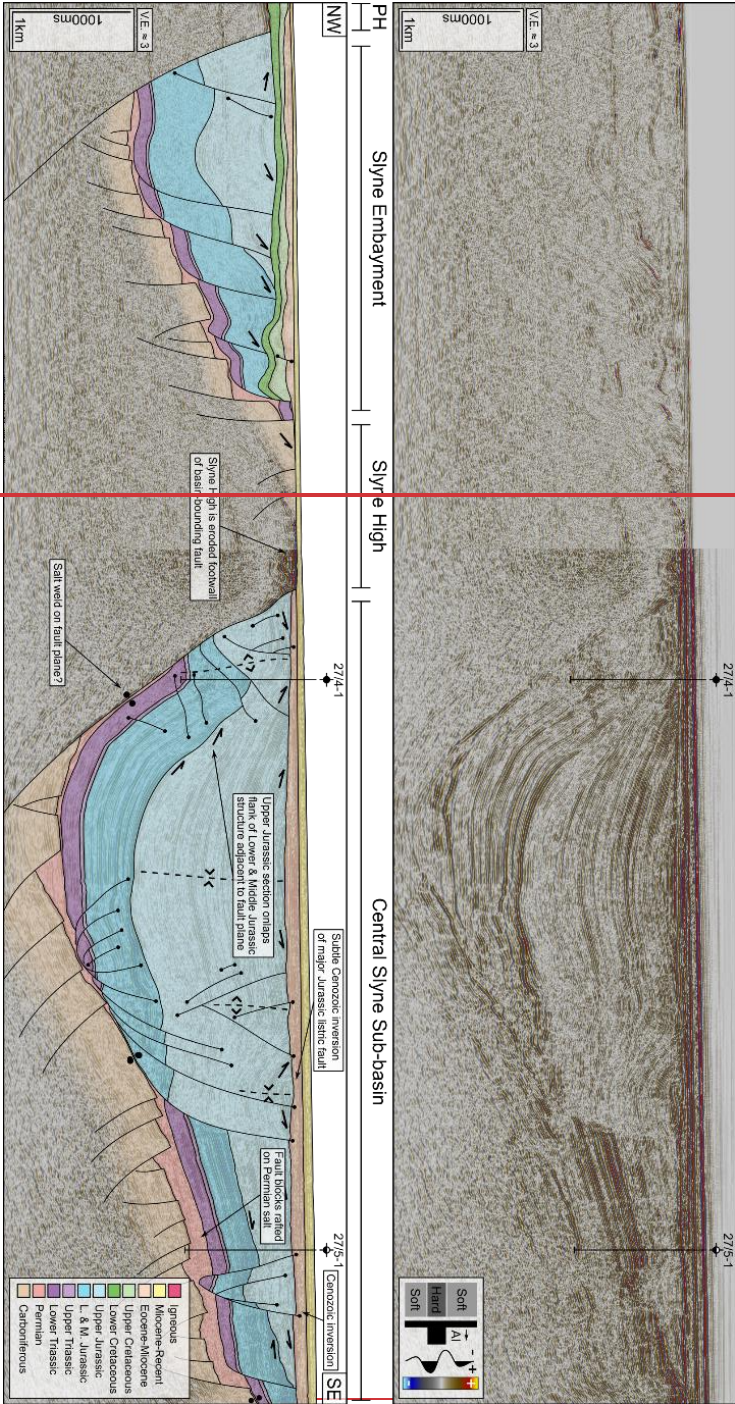
225 5. Results

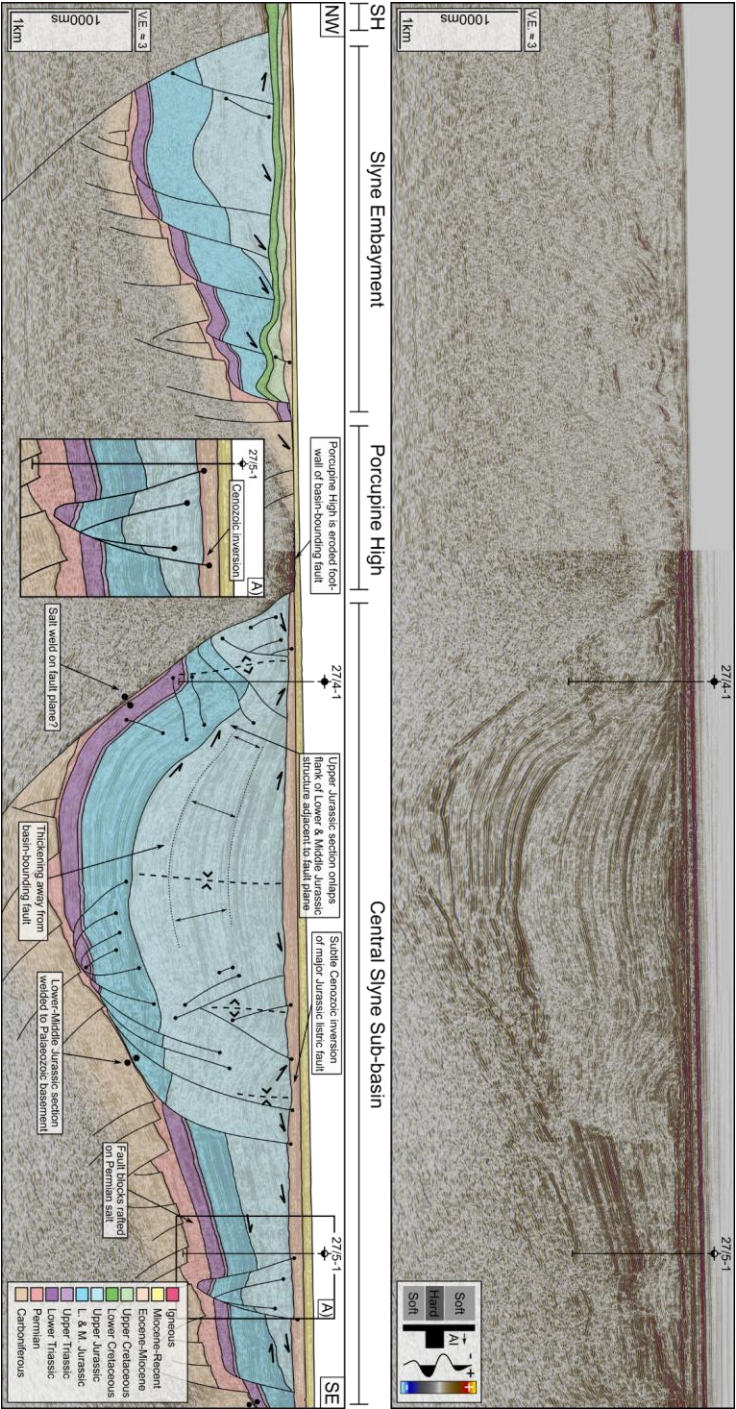
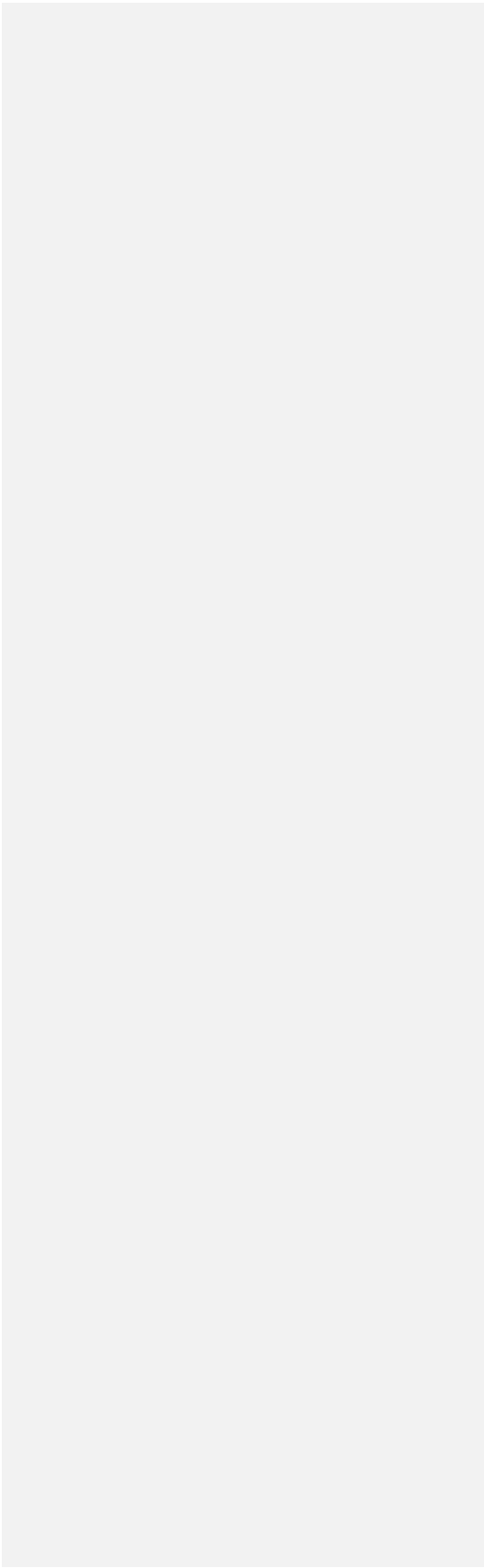
226 5.1. Basin geometry &and transfer zones

227 The Southern and Central Slyne sub-basins are half-grabens which dip towards the northwest
228 (Fig. 4 & 5), with a NNE-SSW oriented basin-bounding fault separating them from the
229 Porcupine High to the west. As no Permian or Mesozoic strata are preserved on the footwall
230 of these basin-bounding faults (the Porcupine High) either through non-deposition or erosion
231 (Fig. 4 & 5), the total throw on these faults is difficult to constrain. Nevertheless, the elevation
232 of the Base-Permian Unconformity in the adjacent hanging wall provides a minimum throw
233 estimate of 3000 ms TWTT (two-way travel time) along most of the length of this fault (Fig.
234 1B). Unlike its Southern and Central neighbours, the Northern Slyne Sub-basin is an eastward-
235 dipping graben (Fig. 6 & 7) bounded by a series of segmented faults along its eastern
236 boundary with the Irish Mainland Shelf (Fig. 1B), while a narrow basement horst separates it
237 from the Rockall Basin to the NW. The fault system bounding the eastern margin of the
238 Northern Slyne Sub-basin consists of a series of left-stepping, NE-SW oriented faults linked
239 by relay ramps (Fig. 1B). These faults are of a similar scale to the fault bounding the Southern
240 and Central sub-basins, with over 3000 ms TWTT of throw recorded (Fig. 1B). The
241 northernmost segment of this fault system separates the Slyne Basin from the Erris Basin to
242 the north, with the Erris Basin being downthrown relative to the Northern Slyne Sub-basin
243 across this fault (Fig. 8).

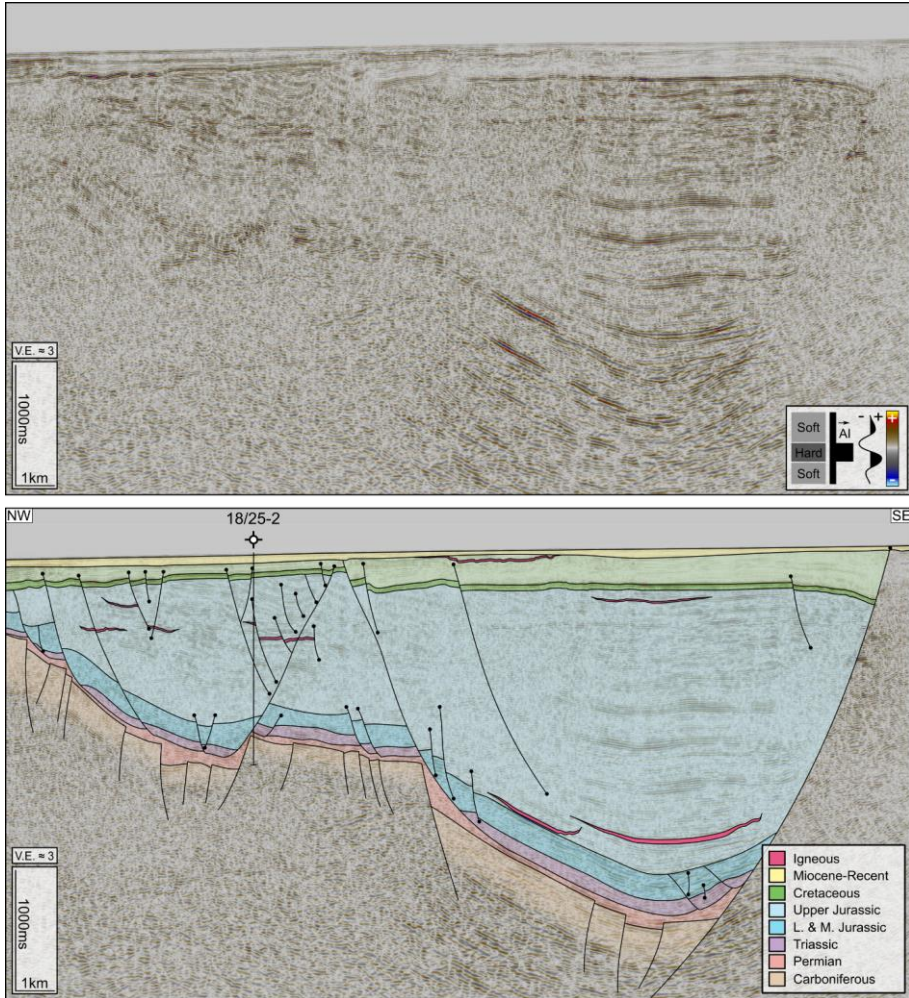


245 **Figure 4:** Composite section of 2D seismic lines NWI-93-202 and NWI-93-028 and
246 accompanying geoseismic interpretation covering the Southern Slyne sub-basin, North
247 Porcupine Basin, and Brendan Igneous Centre. The Southern sub-basin is a westward-
248 dipping half-graben, and is downthrown relative to the North Porcupine Basin, separated by a
249 narrow high composed of crystalline basement. See Figure 1 for location.



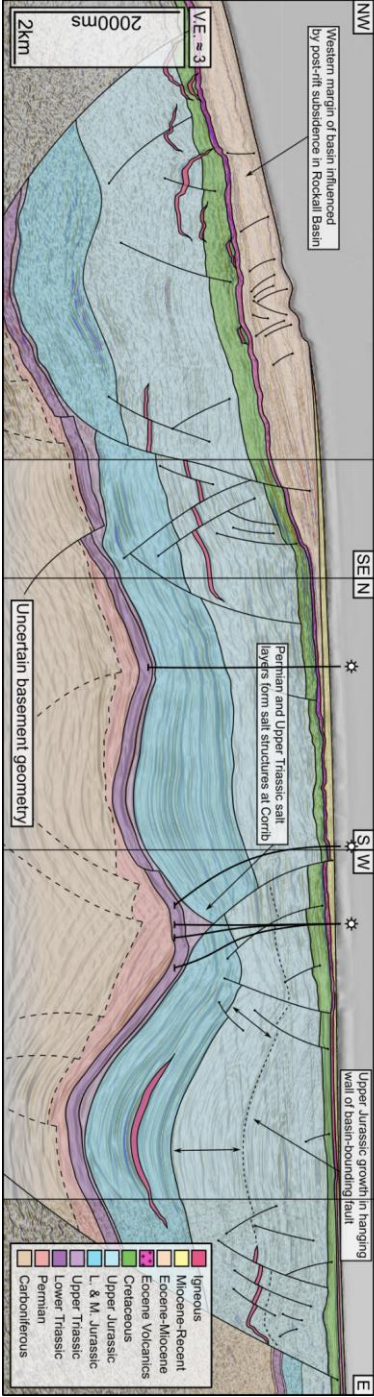
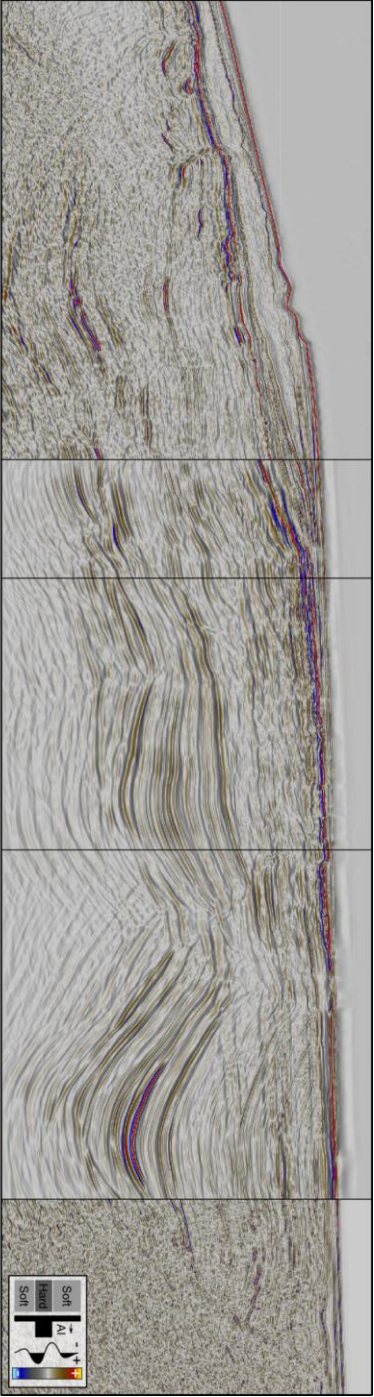


252 **Figure 5:** Composite seismic section of 2D seismic line E961E09- 28 and inline 2740 from the
253 2000/08 (E001E09) 3D seismic volume from the Central Slyne Sub-basin, with accompanying
254 seismic interpretation. See Figure 1 for location. **Abbreviations:** PH – Porcupine High.

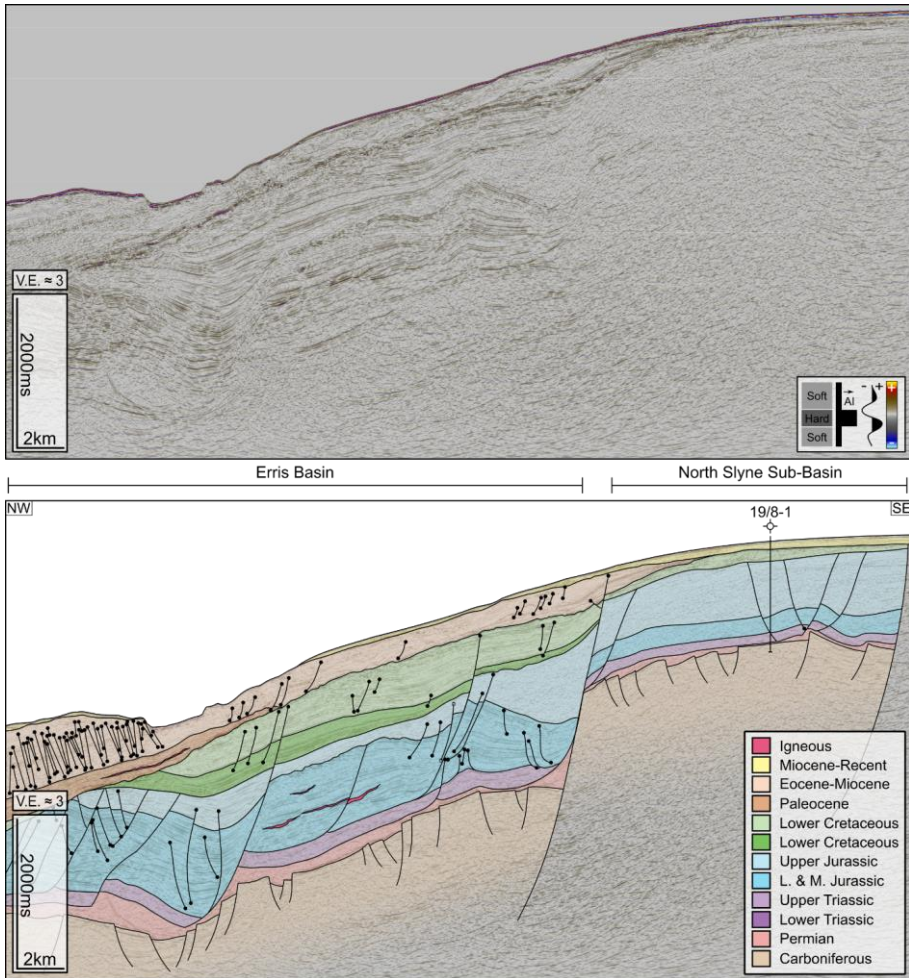


255

256 **Figure 6:** 2D seismic line E931E07 and accompanying geoseismic interpretation from the
 257 Central Slyne Transfer Zone. Basin polarity has switched from the westward-dipping half-
 258 graben geometry of the Central and Southern sub-basins to an eastward-dipping half-graben
 259 geometry. The presence of near-seabed Upper Cretaceous Chalk causes a significant
 260 reduction in image quality. See Figure 1 for location.



262 **Figure 7:** Composite section of an arbitrary line from the Iniskea 2018 3D volume and 2D
263 seismic line ST9808-1002 from the Northern Slyne sub-basin, and accompanying geoseismic
264 interpretation. Significantly thicker Zechstein salt in this part of the Slyne Basin forms salt-
265 pillows and salt-anticlines, folding the overlying Mesozoic section. Detachment on the Uilleann
266 Halite causes rafting and listric faulting in the overlying Jurassic section. See Figure 1 for
267 location. **Abbreviations:** ER – Erris Ridge.



268

269 **Figure 8:** 2D seismic line ST9505-430 and accompanying geoseismic interpretation covering
 270 the Northern Slyne sub-basin and the southern Erris Basin. The Erris Basin is downthrown
 271 relative to the Slyne Basin, and has a significantly thicker Lower and Middle Jurassic
 272 preserved, but conversely reduced Upper Jurassic stratigraphy. Significantly thicker
 273 Cretaceous and Cenozoic post-rift stratigraphy is preserved in the Erris Basin relative to the
 274 Slyne Basin. See Figure 1 for seismic line location.

275 The reversal of basin polarity occurs across the CSTZ, which coincides with the intersection
 276 of the offshore extension of the GGFZ and the Slyne Basin- (Fig. 1B). Deep seismic transects
 277 adjacent to the Slyne Basin image the GGFZ as a NE-SW trending vertical discontinuity which
 278 appears to offset the Moho (Klemperer et al., 1991). The throw on the basin-bounding faults
 279 north and south of the CSTZ rapidly decreases as they approach the CSTZ so that horizons
 280 are continuous between the basins and strain is transferred between the faults of opposed

281 polarity via a convergent, conjugate transfer zone (sensu Morley et al., 1990). Both faults have
282 over 3000 ms TWTT of throw on the Base Permian Unconformity within 10 kilometres of the
283 CSTZ (Fig. 1, 5, 6), with this value likely being an underrepresentation of the true throw given
284 the kilometre-scale erosion of Jurassic sediments recorded both north and south of the CSTZ
285 beneath the post-rift unconformities (e.g. Corcoran & Mecklenburgh, 2005; Biancotto et al.,
286 2007). In addition to the faults bounding the Central and Northern Slyne sub-basins, a NE-SW
287 oriented, southward dipping fault bounds the Slyne Embayment, a small half-graben to the
288 southwest of the CSTZ (Fig. 1B, 5). This suggests that the GGFZ ~~acted as a barrier to~~ localised
289 the ~~propagation~~ formation of the ~~transfer zone between the~~ basin-bounding ~~fault systems~~ faults
290 to both the north and south. ~~The GGFZ is likely linked to both the fault bounding~~ Pre-existing
291 ~~deformation in the Slyne Embayment and~~ Caledonian-aged basement associated with the
292 ~~southernmost segment of fault system bounding the Northern Slyne Sub-basin, both of which~~
293 ~~are subparallel to this major regional structure~~ likely formed a preferential zone to transfer
294 ~~strain between the younger Permo-Mesozoic faults during these extensional episodes.~~

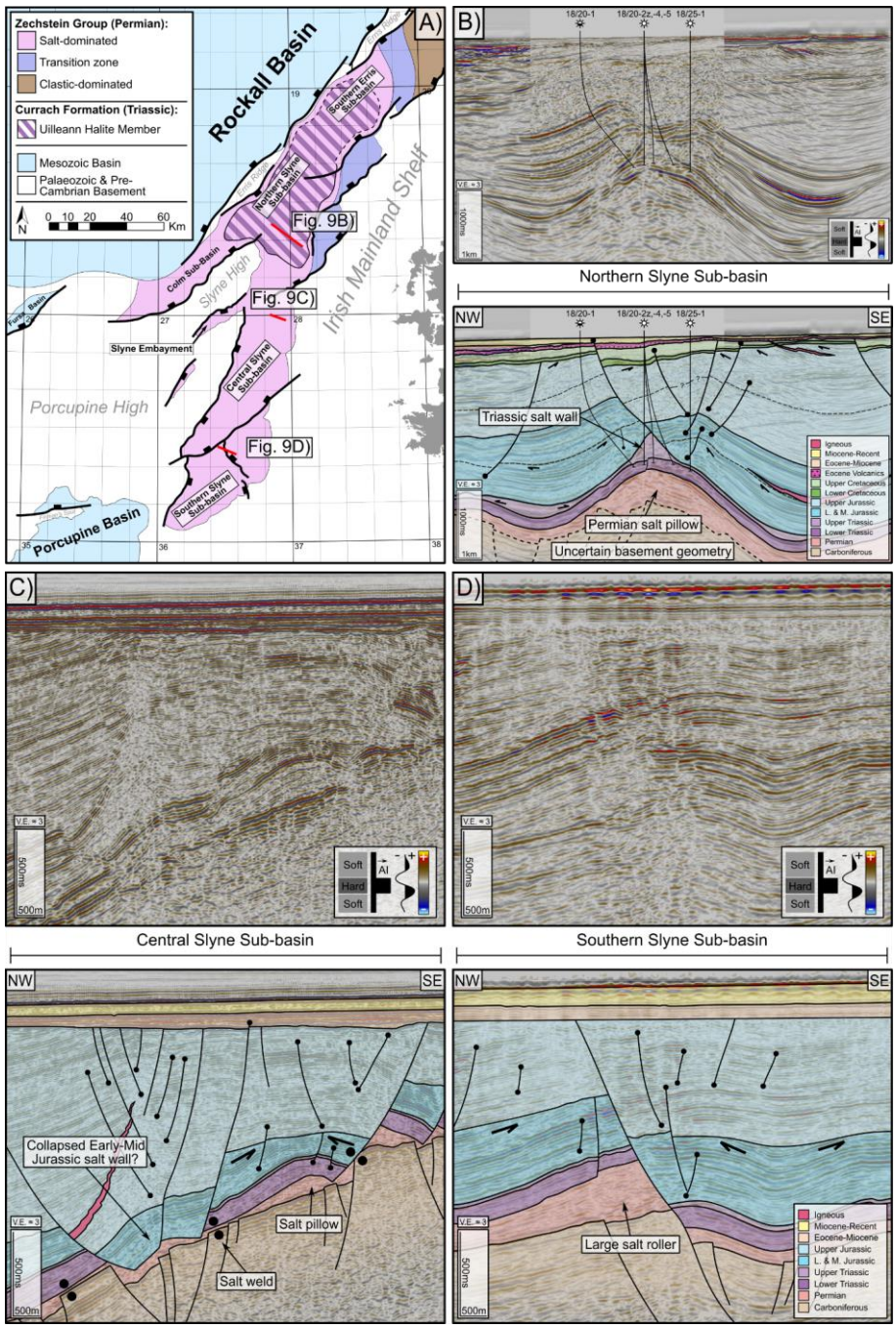
295 The HBFC fault is interpreted as a hard-linked NE-SW oriented fault, dipping towards the NW,
296 which downthrows the Central Slyne Sub-basin relative to the Southern Slyne Sub-basin (Fig.
297 1B). The HBFC fault also appears to offset the NNE-SSW oriented fault bounding the Central
298 and Southern Slyne sub-basins ~~with a sinistral sense of motion~~ (Fig. 1B), ~~which~~. This map-
299 ~~view shape~~ may be a product of both normal dip-slip movement ~~observed offshore on seismic~~
300 ~~data and, preserving more of the syn-rift basin beneath the post-rift unconformity in the~~
301 ~~hanging wall of the HBFC fault and sinistral~~ strike-slip movement recorded onshore Ireland
302 (e.g. Worthington & Walsh, 2011; Anderson et al., 2018). The nature of the interaction between
303 these two faults is unclear due to poor seismic image quality caused by shallow Cenozoic
304 lavas which blanket the western margin of the Southern Slyne Sub-basin. However, the lateral
305 offset of the NE-SW oriented basin-bounding fault and the adjacent Porcupine High either side
306 of the ~~FHCB~~ HBFC fault is well imaged on seismic sections immediately north and south of
307 this zone.

308 5.2. The role of salt in basin development

309 The Slyne Basin contains two layers of salt; the Permian Zechstein Group and the Upper
310 Triassic Uilleann Halite Member (Fig. 29A; Dancer et al., 2005; Merlin Energy Resources
311 Consortium, 2020; ~~Fig. 2~~). The Zechstein Group is composed predominately of halite and
312 gypsum, while the Uilleann Halite Member is composed predominantly of halite interbedded
313 with red mudstone and anhydrite (O'Sullivan et al., 2021).

314 In the Central and Southern sub-basins, south of the CSTZ, only the Zechstein Group salt is
315 present (Fig. 2), where it mechanically detaches the sub-salt basement from the Mesozoic

316 supra-salt basin-fill (Fig. 4-5, 9, 10). Several halokinetic structures are present in the Central
317 and Southern Slyne sub-basins, including large salt rollers, collapsed diapirs and rafted fault
318 blocks (Fig. 5, 9). There are also several high-relief monoclines adjacent to the basin-bounding
319 fault in the Central Slyne Sub-basin which have been noted by previous authors (Fig. 5;
320 Dancer et al., 1999). The Triassic and Lower-Middle Jurassic section in these structures is
321 encountered at a similar depth to the same section along the eastern margin of the basin, and
322 the Triassic section appears to have welded to the crystalline basement of the Porcupine High
323 across the fault plane of the basin-bounding fault (Fig. 5). These structures likely formed
324 initially as forced folds above the sub-salt basin-bounding faults during the early stages of
325 rifting in the Late Jurassic, resulting in the Upper Jurassic section onlapping the flank of these
326 structures. As extension continued the fault breached the salt and led to the present geometry
327 (O'Sullivan et al., 2021).



329 **Figure 9:** Seismic sections and accompany interpretations showing salt structures in the Slyne
330 Basin. **A)** Map showing the distribution of Upper Triassic and Permian salt in the Slyne Basin.
331 Adapted from O'Sullivan et al., 2021. **B)** Seismic and geoseismic section through the Corrib
332 gas field showing the kinematic interaction between Upper Triassic and Permian salt. The
333 Permian salt forms a NE-SW oriented salt pillow, while the Upper Triassic forms an elongate
334 salt wall parallel to the fold-axis of the salt pillow. Adapted from O'Sullivan & Childs, 2021. **C)**
335 Several salt-related structures in the Central Slyne Sub-basin, including a salt pillow, salt roller
336 and an apparent collapsed salt diapir. **D)** A large salt roller from the Southern Slyne Sub-basin.
337 The fault in the supra-salt section appears to have hard-linked with the sub-salt basement
338 fault.

339 In the Northern sub-basin both the Permian and Upper Triassic salt layers are present (Fig.
340 9A; Corcoran & Mecklenburgh, 2005; O'Sullivan et al., 2021). Here, both layers mechanically
341 detach the stratigraphy above and below them, with the Permian salt detaching the Lower
342 Triassic from the Carboniferous basement, while the Upper Triassic salt detaches the Jurassic
343 section from the Lower Triassic (Fig. 7, 9B). Halokinetic structures formed in the Permian and
344 Triassic salts are often coincident and can be demonstrated to be kinematically related. This
345 is exemplified by the structure containing the Corrib gas field (Fig. 7, 9; Corcoran &
346 Mecklenburgh, 2005; Dancer et al., 2005); here, the Permian salt forms a NE-SW trending
347 salt pillow, which folds the overlying Mesozoic sediments. An Upper Triassic salt wall formed
348 parallel to the fold-axis of the Permian salt pillow and forms the footwall to a listric ~~delamination~~
349 fault which downthrows the folded Jurassic section to the SE (Fig. 7, 9B). The evolution of the
350 Corrib gas field is discussed in detail in O'Sullivan & Childs (2021).

351 Several of the halokinetic structures in the Slyne Basin record several discrete periods of
352 growth and development. There is significant evidence for halokinesis during the Early and
353 Middle Jurassic, with the crests of fault-blocks cored by salt rollers eroded by the base-Upper
354 Jurassic Unconformity- (e.g. Fig. 9C-D). There is also evidence for Permian salt diapirs
355 forming in the Central Slyne Sub-basin during the Early to Middle Jurassic which collapsed
356 during the Late Jurassic extensional episode, as recorded in the reduced Lower and Middle
357 Jurassic section observed in narrow fault-bounded grabens (e.g. Fig. 9C; Vendeville &
358 Jackson, 2001; O'Sullivan et al., 2021). Several other halokinetic structures were also
359 reactivated during Late Jurassic extension, including the structure containing the Corrib gas
360 field, with significant Late Jurassic throw recorded on the listric fault above the Triassic salt
361 wall (Fig. 9B). Some of these salt structures have also undergone minor modification during
362 the Cretaceous and Cenozoic. Post-rift modification of salt structures was relatively minor
363 compared to deformation associated with the Upper Jurassic phase of rifting, with offsets of
364 c. 10-100 ms TWTT observed on post-rift surfaces (e.g. Fig. 5, 9C). Some of the salt-related
365 post-rift fault movement is observed on the listric fault above the Corrib structure with a distinct
366 Cretaceous growth sequence recorded in the hanging wall of this fault (Fig. 9B).

367

368 6-5.3. Structural Evolution of the Slyne Basin

369 The observations of basin geometry and salt tectonics presented above are now combined
370 with further structural analysis to understand the evolution of the Slyne Basin. This section is
371 divided into sections which broadly correlate with the main tectonic phases observed in the
372 basin, with three episodes of syn-rift extension in the Permian, Early-Middle Jurassic and
373 Late Jurassic followed by post-rift modification during the Cretaceous and Cenozoic.

374 6-1-5.3.1. Permian and Triassic

375 Post-Variscan extension began in the Slyne Basin during the Late Permian. Several hundred
376 metres of Zechstein halite was deposited throughout the Slyne Basin (Fig. 9A), likely in fault-
377 bounded depocentres (O'Sullivan et al., 2021). The Permian boundaries of the Slyne Basin
378 are poorly understood due to post-Permian halokinesis, but it is clear that the Slyne Basin was
379 an area of active extension, relative to the neighbouring Erris and Porcupine basins, with a
380 thin (10s of metres thick) layer of predominately clastic and carbonate facies developed in the
381 former (Robeson et al., 1988; O'Sullivan et al., 2021), and no evidence of Permian sediments
382 in the latter (Jones & Underhill, 2011; Bulois et al., 2018).

383 The Triassic was a period of relative quiescence in the Slyne Basin, typified by the near
384 isopachous nature of the Lower Triassic section throughout the basin (Fig. 5, 7, 9). The local
385 thickening of the Upper Triassic section in the synclines flanking the Corrib anticline (Fig. 7,
386 9B) suggest that low-strain extension may have begun during the Late Triassic, at least in the
387 Northern Slyne Sub-basin (O'Sullivan & Childs, 2021).

388 6-2-5.3.2. Early and Middle Jurassic

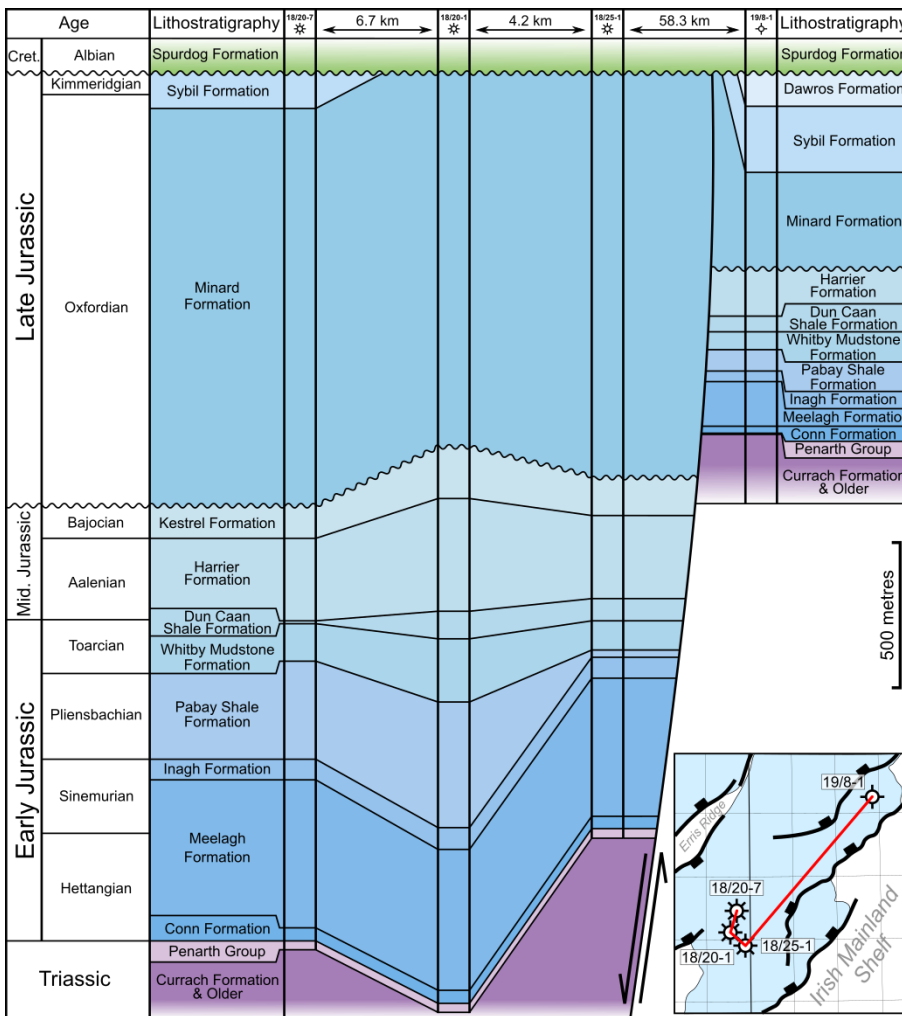
389 Low-strain regional extension occurred throughout the Slyne Basin during the Early and
390 Middle Jurassic. In the Northern Slyne Sub-basin, a comparison of the stratigraphic section
391 encountered in basinward wells with the single available well located on the footwall of the
392 basin-bounding faults demonstrates the growth in the Lower and Middle Jurassic section
393 during this period of regional extension (Fig. 10). ~~The~~ In the Central Slyne Sub-basin the Lower
394 and Middle Jurassic section can be observed thickening towards the basin-bounding faults in
395 the Central Slyne Sub-basin by a few 10s of ms TWTT (10-100 metres, Fig. 11D), but this
396 shape is accentuated by erosion of this section at the Base Upper Jurassic Unconformity on
397 the basin margins (e.g. well 27/5-1 location in Fig. 5). The Lower and Middle Jurassic section
398 is also observed thickening into the synclines flanking the salt-cored folds in the Northern
399 Slyne Sub-basin (Fig. 7, 9B), indicating the Permian salt was undergoing halokinesis during
400 this period (O'Sullivan & Childs, 2021). There is also evidence of salt walls forming in the
401 Central Slyne Sub-basin during the Early to Middle Jurassic along with large salt rollers

Formatted

Formatted

Formatted

402 beneath active listric faults soling out in the Permian Zechstein Group (Fig. 9C, D). 9C, D.
 403 11D). In the Northern Slyne Sub-basin, a comparison of the stratigraphic section encountered
 404 in basinward wells with the single available well located on the footwall of the basin bounding
 405 faults demonstrates the growth in the Lower and Middle Jurassic section during this period of
 406 regional extension (Fig. 10).



407
 408 **Figure 10:** Well correlation through the Jurassic section of key wells from the Northern Slyne
 409 Sub-basin, highlighting thickness variations in the Lower and Middle Jurassic section between
 410 wells within the basin and the 19/8-1 well on the footwall of the basin-bounding fault system.

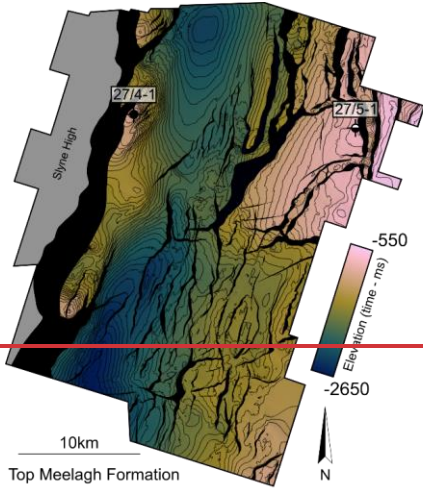
411 A regional unconformity separates the Lower to Middle Jurassic from the Upper Jurassic
 412 section throughout the Slyne Basin, termed the Base Upper Jurassic Unconformity. This

413 unconformity can be quite rugose on the margins of the basins, such as the area around the
414 27/5-1 well in the Central Slyne Sub-basin (Fig. 5), while being a relatively flat paraconformity
415 in the centre of the basin (e.g. Fig. 5, 7). There are several angular truncations observed
416 throughout the Slyne Basin at the base of this unconformity, particularly above salt-related
417 structures formed during Early to Middle Jurassic extension, including footwalls above salt
418 rollers and the crests of folds above salt pillows (Fig. 9C, D). Throughout the Slyne Basin the
419 late Middle Jurassic (Bathonian and Callovian) section is absent at this unconformity, either
420 through erosion or non-deposition (Merlin Energy Resources Consortium, 2020). The exact
421 cause of this unconformity is difficult to constrain, although some authors have suggested
422 thermal doming and dynamic topography above a mantle plume similar to that implicated in
423 the North Sea (Tate & Dobson, 1989; Underhill & Partington, 1993; Doré et al., 1999).

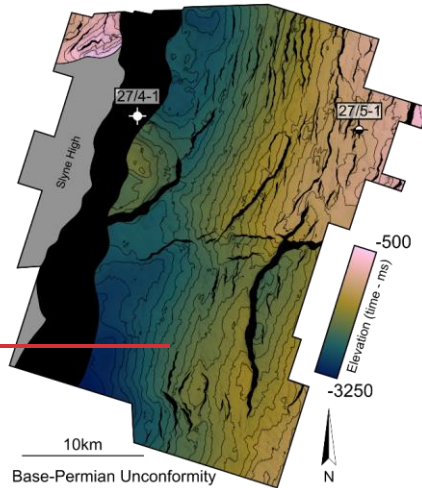
424 6.3.5.3.3. Late Jurassic

425 The main phase of extension commenced during the Late Jurassic, with the basin-bounding
426 faults accumulating several kilometres of throw during this extensional episode along with the
427 deposition of several kilometres of Upper Jurassic sediment (Fig. 4-8). Despite this, there are
428 no obvious growth sequences observed in the Southern Slyne Sub-basin (Fig. 4) or in the
429 southern portion of the Northern Slyne Sub-basin (Fig. 6). Growth sequences are observed in
430 the hanging walls of the bounding faults in the Northern Slyne Sub-basin with reflectors
431 diverging towards the SE (Fig. 7). In the Central Slyne Sub-basin, the Upper Jurassic section
432 onlaps the flank of the high-relief monocline in the immediate hanging wall of the basin-
433 bounding fault and thickens into the hanging wall of major intra-basinal listric fault (Fig. 5).
434 This stratal geometry, along with a similar thickness of Lower-Middle Jurassic sediment
435 present in the neighbouring Slyne Embayment, suggests that most of the ~~throw~~slip on ~~this~~the
436 fault bounding the Central Slyne Sub-basin accumulated during the Late Jurassic, with the
437 kilometre-scale post-rift uplift and erosion during the Cretaceous and Cenozoic removing any
438 Jurassic sediment from the intervening footwall, forming the Slyne High (Fig. 5). The presence
439 of NE-SW oriented fault splays in the sub-salt hanging wall of this fault (e.g. Fig. 11) suggests
440 that the large NNE-SSW oriented fault bounding the Central and Southern Slyne Sub-basins
441 formed through the linkage of NE-SW oriented fault segments, likely during this Late Jurassic
442 phase of rifting.

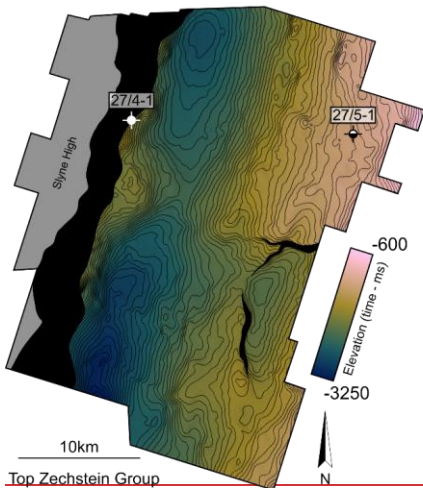
Formatted



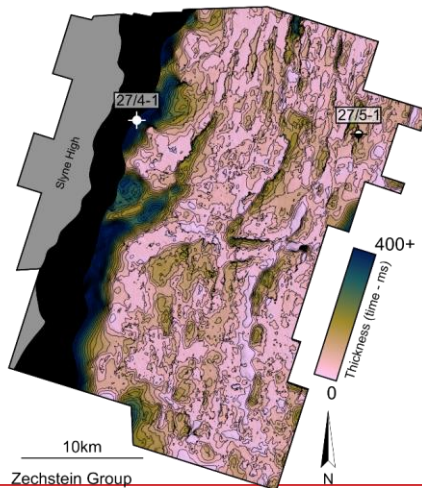
Top Meelagh Formation



Base-Permian Unconformity

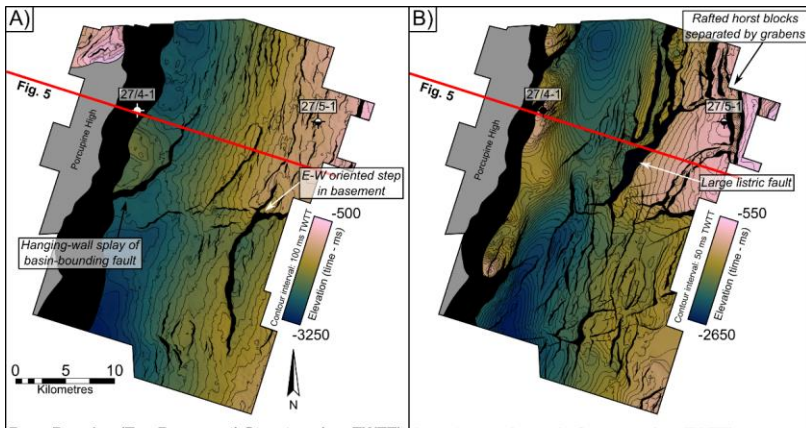


Top Zechstein Group

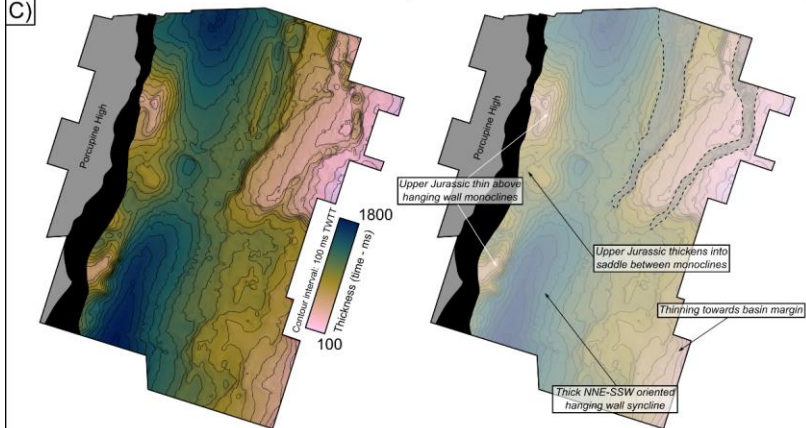


Zechstein Group

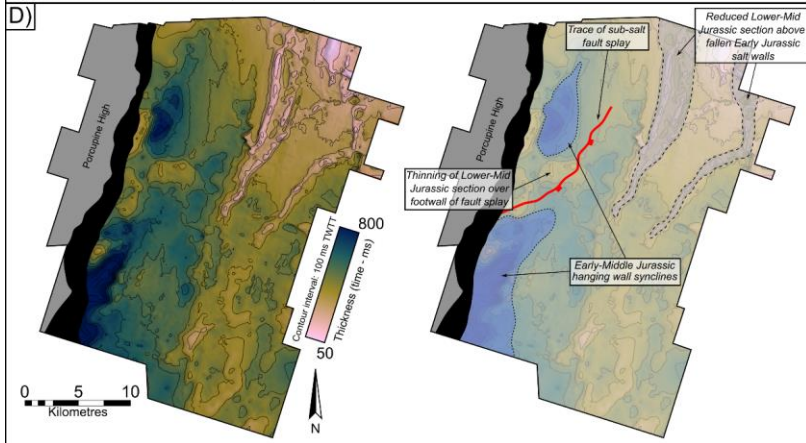
443



Base-Permian (Top Basement) Structure (ms TWTT) Intra-Lower Jurassic Structure (ms TWTT)



Upper Jurassic Thickness (ms TWTT)



Lower-Middle Jurassic Thickness (ms TWTT)

445 **Figure 11:** ~~Surfaces~~Structure maps and thickness maps (in ms TWTT) from the E00IE09 3D
446 seismic volume from the Central sub-basin. See Figure 1 for location. **A)** TWTT structure map
447 of the Variscan Unconformity. **B)** TWTT structure map of the Top Meelagh Formation- (intra-
448 Lower Jurassic). Several high-relief anticlinal closures are present in the immediate hanging-
449 wall of the basin-bounding fault, including the structure containing the 27/4-1 'Bandon' oil
450 accumulation. ~~–B) TWTT structure map of the Variscan Unconformity. Notice~~Note
451 the significant differences in fault pattern between the Variscan Unconformity (pre-salt) and Top
452 Meelagh Formation (post-salt). ~~C) TWTT structure map of the Top Zechstein Group. Notice~~
453 ~~the lack of faulting on this surface.~~ **D)** TWTT thickness map (isochron) of the Zechstein Group.
454 ~~The Zechstein salt is thinned throughout most of the survey area, with numerous apparent~~
455 ~~welds formed between the post- and pre-salt sections. The Zechstein salt is overthickened in~~
456 ~~the immediate hanging wall of the basin-bounding fault.~~ **C)** TWTT thickness map of the Upper
457 Jurassic. Note the thinning of the Upper Jurassic section onto the hanging-wall monoclines,
458 including the structure drilled by the 27/4-1 well. **D)** TWTT thickness map of the Lower and
459 Middle Jurassic. Note the local thickening in the hanging wall of the fault splay in the sub-salt
460 basement, and the thinning in the NE of the surface. This thinning is evidence of Zechstein
461 salt diapirs which were present in the Early-Middle Jurassic, which then collapsed during Late
462 Jurassic extension.

463 Two discrete phases of Late Jurassic extension have been identified in the neighbouring
464 Porcupine Basin, the first occurring in the Oxfordian and the second in the Kimmeridgian
465 (Saqab et al., 2020). Both of these extensional episodes may have also occurred in the Slyne
466 Basin but, unlike the Porcupine Basin, a significant section of the Late Jurassic syn-rift section
467 was subsequently removed during post-rift uplift and erosion (e.g. Corcoran & Mecklenburgh,
468 2005) and evidence of a second phase may have been removed. This may explain the lack of
469 distinct growth-sequences observed in the Upper Jurassic in the Southern Slyne Sub-basin,
470 where movement on the bounding-fault may have occurred in tandem with sedimentation rate
471 during the Oxfordian, followed by more movement occurring during the Kimmeridgian.

472

473 6.4.5.3.4. Cretaceous and Cenozoic

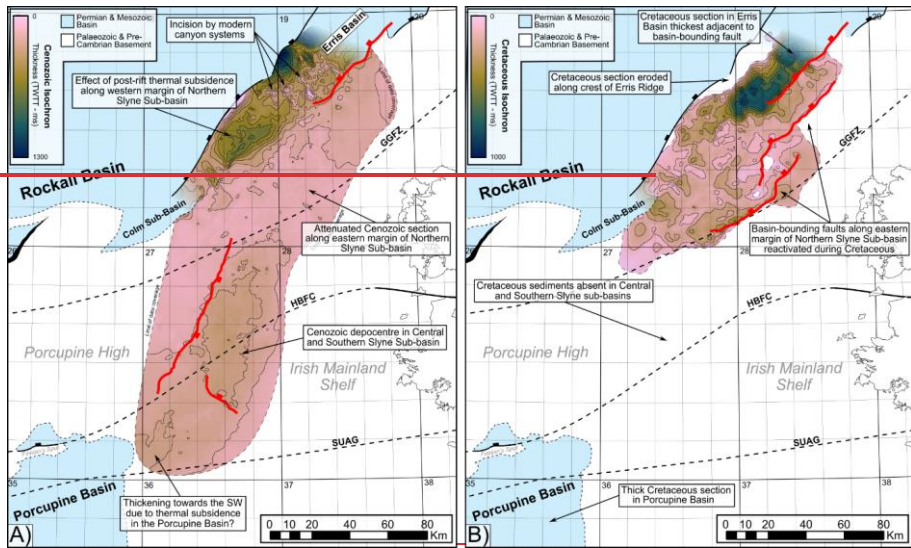
474 The Slyne Basin experienced kilometre-scale uplift and erosion at the end of the Jurassic and
475 during the Early Cretaceous, removing a significant section of the Upper Jurassic syn-rift
476 section throughout the basin (Table 1). The majority of the Slyne Basin was likely a
477 topographic high relative to surrounding regions during the Cretaceous, including the Erris,
478 Porcupine and Rockall basins (Fig. 8; Musgrove & Mitchener, 1996; Chapman et al., 1999;
479 Saqab et al., 2020). Up to 400 metres of Albian and Late Cretaceous sediments were
480 deposited in the Northern Slyne Sub-basin and the Slyne Embayment (5-8, 12B), and possibly
481 in the Central and Southern Slyne sub-basins. Several faults active during the Late Jurassic
482 syn-rift fault phase were reactivated during the Cretaceous, with both normal and reverse
483 movement observed throughout the Slyne Basin. In the Northern Slyne Sub-basin the main
484 delamination fault above the Corrib anticline has a significant Cretaceous growth sequence

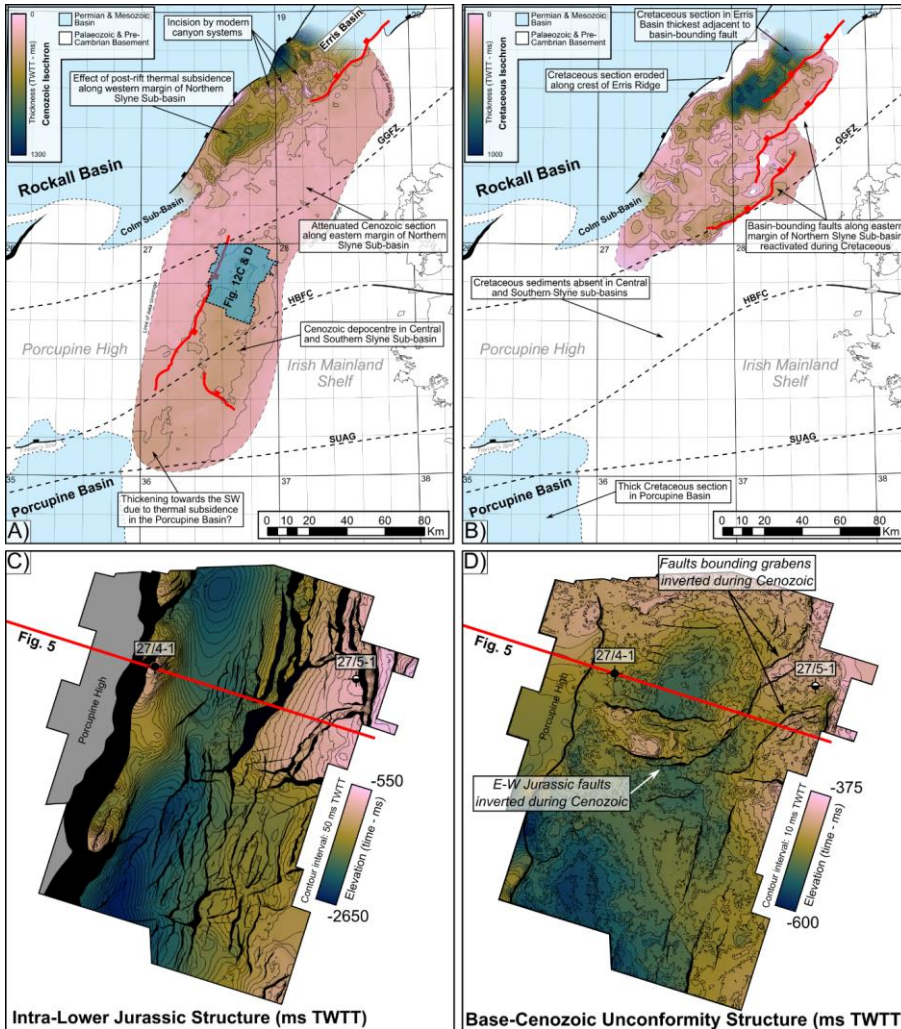
Formatted

485 that thickens from 200 ms TWTT (c. 150 m) in the footwall to over 400 ms TWTT (c. 380 m)
486 in the hanging-wall (Fig. 7). Additionally, the individual segments of the basin-bounding fault
487 system along the eastern margin of the Northern Slyne Sub-basin were reactivated during the
488 Cretaceous (Fig. 12B). The throw on the northern segment varies from 30-100 ms TWTT
489 adjacent to the Corrib gas field through to the 19/8-1 well (Fig. 7, 8) while on the segment to
490 the south adjacent to the 18/25-2 well (Fig. 6) the throw locally exceeds 300 ms TWTT. In
491 addition to these major faults, several smaller faults offset the Cretaceous section throughout
492 the Northern Slyne Sub-basin with the majority of these ~~fault~~structures having throws less
493 than 100 ms TWTT (Fig. 6, 7). The fault bounding the Slyne Embayment appears not to have
494 been active during this time, with Cretaceous sediments overstepping the fault with no offset
495 (Fig. 5). The absence of Cretaceous sediments in the Central and Southern Slyne sub-basins
496 obscures any fault activity that may have occurred during this period (Fig. 12B). Nevertheless,
497 due to the pervasive nature of Cretaceous faulting in the Northern Slyne Sub-basin and strong
498 evidence of Cretaceous faulting in the Porcupine Basin to the southwest (Jones & Underhill,
499 2011; Saqab et al., 2020), it is likely that some structures in the Central and Southern Slyne
500 sub-basins were active during the Cretaceous. The motion on these faults would likely have
501 been less than 100 ms TWTT in a similar manner to those in the Northern Slyne Sub-basin.
502 Alongside the reactivation of Late Jurassic syn-rift faults, the majority of which were oriented
503 NNE-SSW parallel to the axis of the Slyne Basin, a new set of ENE-WSW oriented faults
504 formed during the Cretaceous, observed offsetting the upper 100-200 ms TWTT of the Upper
505 Jurassic section and the Cretaceous section in the Northern Slyne Sub-basin (O'Sullivan &
506 Childs, 2021).

Exhumation estimate (Km)	Location	Source
0.7-1.9	27/13-1	Scotchman & Thomas, 1995
0.8-1.7	Corrib	Corcoran & Mecklenburgh, 2005
0.7-3.2	Central and Southern Slyne sub-basins	Biancotto & Hardy, 2007
1.6-2.0	27/24-sb02	Fugro, 1994b
1.8	27/5-1	Geotrack, 1996
0.8-2.6	19/8-1	Geotrack, 2008

507 **Table 1:** Exhumation estimates from different locations throughout the Slyne Basin. Well
508 locations are shown in Figures 1 and 3.





510
 511 **Figure 12: A)** TWT thickness map (isochron) of the Cenozoic section in the Slyne and
 512 southern Erris Basins superimposed on the **main**-syn-rift structural features. A thicker Cenozoic
 513 section is observed along the margin of the Rockall Basin on the western margin of the
 514 Northern sub-basin and in the southern Erris Basin. This is transected by modern slope
 515 canyons which incise into the Cenozoic section. A thicker Cenozoic section is also observed
 516 in the Central sub-basin. **B)** TWT thickness map (isochron) for the Cretaceous section in the
 517 Slyne and southern Erris Basins superimposed on the **main**-syn-rift structural features.
 518 Cretaceous strata are absent in the Slyne Basin south of the Central Slyne Transfer Zone but
 519 is present in the North Porcupine Basin. A significantly thicker Cretaceous section is preserved
 520 in the southern Erris Basin, although it is eroded along the north-western margin of the Erris
 521 Basin. **C)** TWT structure map of the Intra-Lower Jurassic in the Central Slyne Basin. **D)** TWT
 522 structure map of the Base-Cenozoic Unconformity in the Central Slyne Sub-basin. Notice the

523 subtle inversion structures, including a WNW-ESE block in the centre of the map and small
524 grabens around the 27/5-1 well.

525 A second period of uplift and erosion occurred during the early Cenozoic throughout the Slyne
526 Basin, forming another regional unconformity (Fig. 4-8). This was accompanied by a period of
527 regional magmatism, expressed as igneous intrusions observed throughout the Slyne Basin
528 (Fig. 4, 6, 7, 8) and layers of basaltic lava in the Northern and Southern Slyne sub-basins (Fig.
529 4, 7).

530 Cenozoic tectonic activity reactivated several structures throughout the Slyne Basin with
531 different expressions and senses of motion in different sub-basins; In the Northern Slyne Sub-
532 basin the delamination fault above the Corrib anticline was reactivated for a second time,
533 offsetting the early Eocene lavas of the Druid Formation, alongside the large listric fault to the
534 west of Corrib (Fig. 7). In the Central and Southern Slyne sub-basins, several intra-basinal
535 faults were reactivated, with both normal and reverse motion observed on faults with Cenozoic
536 throw between 10 to 50 ms TWTT (Fig. 5, 12D). The large listric fault in the Central Slyne-Sub
537 basin was inverted along with some of the rafted fault blocks along the eastern margin of the
538 basin (Fig. 5, 12D). In the Central Slyne Sub-basin the bounding fault along the western
539 margin of the basin was ~~reactived~~reactivated during the Cenozoic, with between 50-150 ms
540 TWTT of throw recorded along its length (Fig. 5, 12A). The faults bounding the Northern Slyne
541 Sub-basin were not reactivated during the Cenozoic (Fig. 6-8, 12A) but due to thermal
542 subsidence in the neighbouring Rockall Basin the Cenozoic sequence thickens significantly
543 along the western margin of the Northern Slyne Sub-basin (Fig. 7, 8, 12A).

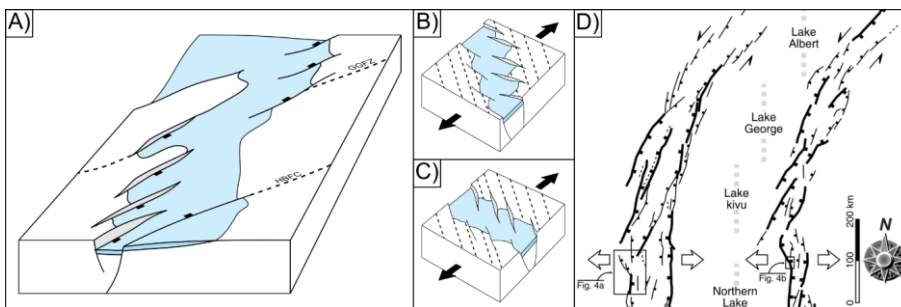
544 7.6. Discussion

545 7.4.6.1. Structural inheritance and the impact of oblique pre- 546 existing structures

547 Structural inheritance is a common feature across the sedimentary basins of NW Europe, with
548 Carboniferous, Permian, Jurassic and Cretaceous rifting interpreted to reactive older, pre-
549 existing structures which formed during the Caledonian or Variscan Orogenies. This is
550 recorded along the Atlantic margin of NW Europe (Stein, 1988; Doré et al., 1999; Ziegler &
551 Dèzes, 2006; Schiffer et al., 2019) as well as in the basins of the North Sea (Fazlikhani et al.,
552 2017; Philips et al., 2019; Osagiede et al., 2020). The reactivation of structures has been
553 observed both onshore and offshore Ireland, with faults in the Carboniferous basins in the Irish
554 midlands forming parallel to the NE-SW structures in the Caledonian basement (Worthington
555 & Walsh, 2011; Kyne et al., 2019), while Variscan structures form the template for the later
556 development of the Celtic Sea basins (Van Hoorn, 1987; Shannon, 1991; Rodriguez-Salgado

557 et al., 2019). Similar relationships have been suggested for the Irish Atlantic margin (Tate &
558 Dobson, 1989; Naylor & Shannon, 2005), with several Caledonian structures mapped onshore
559 continuing into the offshore domain (Fig. 1).

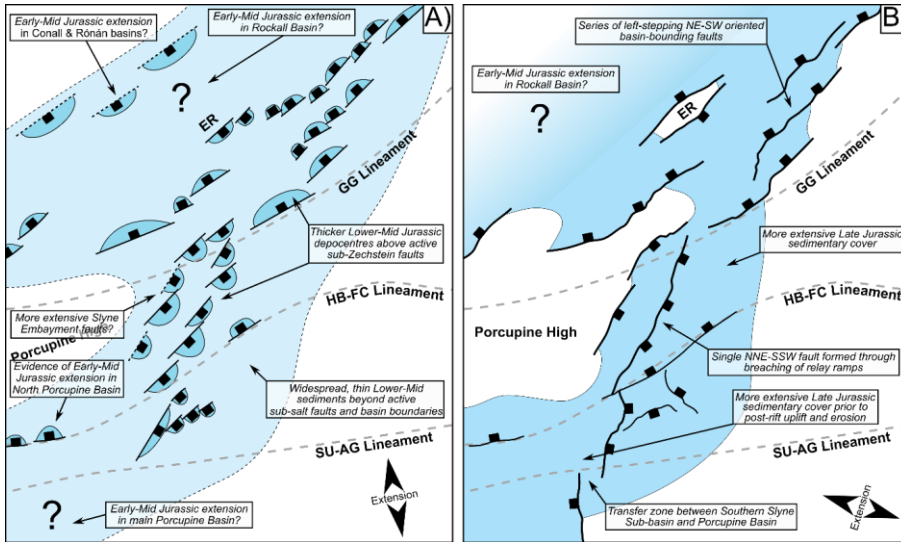
560 The relationship between pre-existing basement structure and basin formation has been
561 studied extensively from outcrop and subsurface mapping and using analogue modelling (e.g.
562 Tommasi & Vauchez, 2001; Fazlikhani et al., 2017; Collanega et al., 2019). The key factor
563 that determines the nature of this relationship is the relative orientation of inherited structure
564 and the later extension direction (e.g. Henza et al., 2011; Henstra et al., 2015). Where
565 inherited structures are at a low angle to the extension direction, they are not reactivated but
566 may impede the propagation of new extensional faults and may give rise to transfer zones
567 between adjacent fault/basin segments. As the angle between pre-existing structures and
568 extension direction increases the likelihood of reactivation of basement structure increases
569 and analogue modelling has demonstrated the variety of fault patterns that can form in the
570 cover sequence. Although the effect of basement structure can be manifest in many ways the
571 two situations that have received most attention are extension oblique to an individual
572 basement fault (Schlishe et al., 2002) and oblique basin opening modelled by extension
573 oblique to a zone of weakness (Agostini et al., 2009; Philippon & Corti, 2016). In both cases
574 extension results in the formation of new fault segments, or faults, that are normal, or close to
575 normal, to the extension direction and arranged en echelon above or within the basement
576 structure or zone. Figure 13B illustrates fault/basin geometry that is characteristic of extension
577 oblique to a basement fabric; the key feature is that the overall orientation of the **structurebasin**
578 is parallel to the basement structure **while individual faults may not align with these basement**
579 **structures**. The Slyne Basin does not follow Caledonian basement structure but cuts across it
580 and as a result displays a different style of inheritance. Figure 13A **illustratesand 14A illustrate**
581 our interpretation of the initial Jurassic geometry of the Slyne Basin that is based on
582 observations below; this geometry resembles that in Fig. 13C in which individual fault
583 segments follow the basement **trendstructures** but the basin as a whole cuts across it.



584

585 **Figure 13: A)** Schematic block model showing the initial fault segments of the basin bounding
586 faults and the reversal in basin polarity across the GGFZ. **B-C)** Blocks models showing
587 different patterns of basement formation when extension is oblique to pre-existing structures.
588 ~~D) Section of Figure 3 of Corti et al. Dashed lines represent pre-existing structures, white~~
589 ~~polygons represent active faults, and blue polygons represent the actively forming rift basin.~~
590 ~~B) Basin orientation matches pre-existing structures while active faults crosscut them. C)~~
591 ~~Active faults match pre-existing structures while the basin crosscuts them D) Section of Figure~~
592 ~~3 of Corti et al. (2007) demonstrating similar rift geometries to those observed in the Slyne~~
593 ~~Basin.~~

594 The Slyne Basin strikes NNE-SSW (020°) and cuts across the local Caledonian inherited trend
595 oriented NE-SW (c. 045°). On the eastern flank of the Northern Slyne Sub-basin the bounding
596 faults parallel the Caledonian trend and form a left stepping fault array (Fig. 1). The map
597 pattern on the western flank is somewhat obscured by erosion and data quality but the faults
598 also parallel the Caledonian trend. Within the Central Slyne Basin the faults offsetting the
599 Jurassic are predominantly parallel to the basin axis (Fig. 11A). The majority of these faults
600 are confined to the Jurassic section and are decoupled from the Carboniferous basement by
601 the Zechstein salt (Fig. 5). The fault forming the western flank of the Central Slyne Basin is
602 approximately parallel to the basin trend (Fig. 1) but closer inspection (Fig. 11A) shows that it
603 has a distinct splay in the sub-salt basement. This fault pattern is consistent with this margin
604 of the basin originating as a left-stepping fault array that would have comprised fault segments
605 parallel to the preserved splays i.e. at a strike of ca. 040° and close to the orientation of the
606 Caledonian basement fabric. We suggest therefore that the main faults that bound the Slyne
607 Basin during Jurassic extension initially comprised left stepping arrays of fault segments that
608 individually followed the Caledonian NE-SW trend (Fig. 13A, 14). This initial segmentation is
609 preserved in the fault array bounding the eastern margin of the North Slyne Sub-basin but was
610 bypassed by the formation of a through-going, basin-parallel (i.e. NNE-SSW oriented) fault in
611 the Central Slyne Sub-basin. ~~One of the main Caledonian structures that transects the basin,~~
612 ~~the Great Glen Fault Zone, was one of the structures reactivated to form a segment of the~~
613 ~~eastern margin of the North Slyne Basin and also perhaps one of the segments of the western~~
614 ~~margin of the Central Slyne Basin (the bounding fault of the Slyne Embayment), acted as the~~
615 ~~zone across which the basin reversed polarity. The reason for the different style of basin-~~
616 ~~bounding fault evolution observed either side of the GGFZ is difficult to assess with current~~
617 ~~data. Some potential reasons may be the change in orientation of Caledonian structures from~~
618 ~~NE-SW to E-W towards the south, or the varying composition of the Lewisian and Dalradian~~
619 ~~basement located north and south of the GGFZ respectively.~~



620
 621 **Figure 14:** Conceptual maps showing the evolution of the main basin-bounding and intra-
 622 basinal faults in the Slyne Basin and surrounding areas during the **A)** Early to Middle Jurassic
 623 and **B)** Late Jurassic.

624 The Slyne Basin provides an example of a form of basement control that is not frequently
 625 documented in the literature. In general, individual faults are sub-perpendicular to the
 626 extension direction, whether they be segments of a fault located above a reactivated basement
 627 structure or faults within an oblique rift. The Slyne Basin cuts across the basement trend but
 628 the individual basin bounding faults follow the basement trend. These two styles of interaction
 629 are compared in Figure 13B and 13C. A key difference between these is that there is a reversal
 630 of the sense of stepping of the basin bounding faults despite the fact that the angular
 631 relationship between the basement and the extension direction is the same. This style of
 632 inheritance is not generally recognised in analogue modelling, but Corti et al. (2007) generated
 633 this pattern by introducing discrete narrow zones of weakness (Fig. 13D). Their model,
 634 designed to replicate the structure of the western branch of the East African Rift System,
 635 generated left-stepping rift-bounding faults in the presence of E-W extension by reactivation
 636 of discrete crustal structures in a pattern very similar to that seen in the Slyne Basin. While
 637 this style of inheritance is perhaps unusual, there are other areas in which it can be observed.
 638 In the northern North Sea, a Triassic-Jurassic broadly N-S rift system formed on crust with
 639 both N-S and NE-SW oriented Devonian and Caledonian crustal structures display a wide
 640 variety of styles of inheritance (Fazilkhani et al. 2017; Phillips et al. 2019) but a common
 641 feature is that major faults that parallel Caledonian trends are left stepping and the map pattern
 642 of the Viking Graben, for example, is similar to that of the East African Rift shown in Fig.13D.

643 7-2.6.2. Post-rift uplift and erosion

644 A significant section of the syn-rift section is absent from the Slyne Basin, with key structural
645 geometries recorded in the Upper Jurassic syn-rift sequences missing due to kilometre-scale
646 uplift and erosion during the Cretaceous and Cenozoic (Table 1). The magnitude of uplift and
647 erosion throughout the Slyne and Erris basins is highly variable. Previous authors have
648 recorded a wide range of values for the magnitude of this post-rift exhumation, ranging from a
649 few hundred metres to several kilometres (Scotchman & Thomas, 1995; Corcoran & Clayton,
650 2001; Doré et al., 2002; Corcoran & Mecklenburgh, 2005; Biancotto et al., 2007). This
651 variability in exhumation estimates arises due to the geological complexity associated with this
652 process; in the Slyne Basin, three discrete post-rift unconformities are observed: the Base-
653 Cretaceous, Base-Cenozoic and mid-Miocene unconformities. These unconformities are the
654 result a variety of both local and regional tectonic processes, including rift-shoulder uplift
655 associated with rifting and hyperextension in the neighbouring Rockall Basin, the opening of
656 the Bay of Biscay, the development of the Icelandic plume and the North Atlantic Igneous
657 Province, ridge-push at the Mid-Atlantic Ridge, the Alpine Orogeny, and possibly the
658 development of the Brendan Igneous Centre (Fig. 1, 2; Mohr, 1982). Additionally, these
659 unconformities become composite surfaces at different locations within the Slyne basin: the
660 absence of Cretaceous strata in the Central and Southern Slyne Sub-basins (Fig. 12B) may
661 be due to non-deposition, or more likely, the erosion of the thin Cretaceous section, similar to
662 that observed in the Northern Slyne Sub-basin, during the Cenozoic uplift events. The
663 formation of these composite unconformities obscures the reactivation of any syn-rift faults in
664 the Central and Southern Slyne Sub-basins during the Cretaceous, as the circa 100-300 m of
665 erosion at the Base-Cenozoic Unconformity (sensu Corcoran & Mecklenburgh, 2005) is
666 greater than the throw recorded on most of the Cretaceous faults observed in the Northern
667 Slyne Sub-basin (Fig. 6, 7). Finally, the multitude of methodologies used to estimate
668 exhumation varies throughout the basin, and includes vitrinite reflectance (Scotchman &
669 Thomas, 1995; Corcoran & Clayton, 2001), compaction analysis (Corcoran & Mecklenburgh,
670 2005), and analysis of seismic velocities (Biancotto et al., 2007).

671 A further consequence of this extensive and variable erosion during the Cretaceous and
672 Cenozoic is that the present-day boundaries of the basin are not representative of their full
673 extent during the ~~main~~ Upper Jurassic syn-rift period. The Mesozoic rift basins on the Irish
674 Atlantic margin, including the Slyne Basin, were much more extensive prior to uplift and
675 erosion. Consequently, some publications have, as a result, focused on individual basins as
676 separate and different geological entities rather than as residual parts of a complex, margin-
677 wide rift system. Possible reconstructions of the Slyne Basin and neighbouring areas during
678 the Early-Middle and Late Jurassic periods are presented in Figure 14.

679 **7.3.6.3. The Slyne Basin in the context of the Irish Atlantic**
680 **margin**

681 As stated above, the Slyne Basin belongs to a framework of basins which stretch across the
682 Irish Atlantic margin and likely shares aspects of its geological evolution with these other
683 areas. The most similar of these neighbours is the Erris Basin directly north of the Northern
684 Slyne Sub-basin (Fig. 1). The Erris Basin is contiguous with and has a similar sedimentary fill
685 to the Slyne Basin which suggest that both basins underwent a similar geological evolution
686 during the Permian, Triassic and Jurassic periods (Fig. 8). The evolution of the Slyne and Erris
687 basins diverges in the Cretaceous, with the thicker Cretaceous section in the Erris Basin (Fig.
688 8, 12B) indicating it underwent active extension during the Cretaceous alongside the
689 neighbouring Rockall Basin while the Slyne Basin remained largely inactive.

690 The Slyne Basin is separated from the Porcupine Basin by a narrow basement high
691 approximately five kilometres wide (Fig. 4). This high is the eroded footwall of the fault
692 bounding the Southern Slyne Sub-basin, with kilometre-scale erosion largely taking place
693 during the Cretaceous and Cenozoic (Dancer et al., 1999; Biancotto et al, 2007). Restoring a
694 kilometre-scale section of Upper Jurassic stratigraphy would connect the Porcupine Basin with
695 the Southern Slyne Sub-basin, supporting the idea that these basins developed coevally
696 during the Late Jurassic (Fig. 14B). The nearby 26/30-1 well in the Porcupine Basin (Fig. 4)
697 encountered the Upper Jurassic Minard Formation resting unconformably atop the
698 Carboniferous Blackthorn Group (Phillips Petroleum Company, 1982), while the intervening
699 Permian to Middle Jurassic stratigraphy present in the Southern Slyne Sub-basin is absent.
700 While Triassic and Lower Jurassic stratigraphy has been encountered in two wells in the North
701 Porcupine Basin to the north of the Finnian's Spur (Fig. 1B; Bulois et al., 2018; Merlin Energy
702 Resources Consortium, 2020), most wells in the Northern Porcupine Basin encountered
703 Upper Jurassic sediments resting directly atop Carboniferous sediments (Merlin Energy
704 Resources Consortium, 2020). Permian sediments have not been encountered in any well in
705 the Porcupine Basin (Merlin Energy Resources Consortium, 2020). This indicates that the
706 Slyne Basin is the older of the two basins, with extension beginning in the Late Permian with
707 the deposition of several 100 metres of Zechstein Group evaporites (Štolfova & Shannon,
708 2009; O'Sullivan et al., 2021) while the Northern Porcupine likely remained a relative high
709 during the latest Palaeozoic and early Mesozoic. There may be narrow outliers of Permian,
710 Triassic and Early to Middle Jurassic-aged sediments preserved beneath the Late Jurassic
711 sediments further south in the Porcupine Basin, but at present this remains unproven.

712 **8-7. Conclusions**

713 Detailed interpretation of available seismic reflection data in conjunction with borehole and
714 potential-field datasets has delivered an improved understanding of the complex and
715 multiphase structural history of the Slyne Basin.

716 1. The onset of rifting in the Slyne Basin began in the Late Permian, expressed as diffuse
717 extensional faulting accompanied by the deposition of the Zechstein Group evaporites in
718 localised, fault-bounded depocentres. This was followed by tectonic quiescence during the
719 majority of the Triassic and subsequent extension accompanied by localised halokinesis
720 during the Latest Triassic and into the Early and Middle Jurassic. Regional uplift and
721 erosion occurred during the late Middle Jurassic, creating a regional unconformity. The
722 main phase of rifting began in the Oxfordian and continued until the end of the Jurassic.

723 2. The Slyne Basin experienced kilometre-scale uplift and erosion throughout the Early
724 Cretaceous, creating the distinct angular unconformity between Jurassic syn-rift
725 sediments and Cretaceous and younger post-rift sediments. Subsequent and less-severe
726 phases of exhumation occurred during the Cenozoic. Faults throughout the basin are
727 reactivated in both normal and reverse senses during this tectonic activity.

728 3. Salt layers in the Slyne Basin exert important controls on basin-development, most
729 importantly acting as décollements between the Palaeozoic pre-salt basement and
730 Mesozoic post-salt basin-fill. The most important salt-prone interval is the Permian
731 Zechstein Group, present throughout the Slyne Basin, while in the Northern sub-basin the
732 Upper Triassic Uilleann Halite Member is also present, acting as a second layer of
733 mechanical detachment.

734 3.4. The segmentation of the Slyne Basin into discrete sub-basins occurs where crustal-
735 scale structural lineaments, representing the suture zones and boundaries between
736 Caledonian and Precambrian terranes, obliquely transect the younger Mesozoic basin.

737 4.5. The basin axis is oriented NNE-SSW and cuts across the N-E Caledonian trend
738 resulting in a rarely documented style of fault reactivation in which the segments of basin-
739 bounding faults follow the earlier structural grain but the basin as a whole does not. As
740 strain increased initial left-stepping segments linked resulting in basin-bounding faults
741 oriented parallel to the basin axis.

742 ~~5.1. Salt layers in the Slyne Basin exert important controls on basin development, most~~
743 ~~importantly acting as décollements between the Palaeozoic pre salt basement and~~
744 ~~Mesozoic post salt basin fill. The most important salt prone interval is the Permian~~
745 ~~Zechstein Group, present throughout the Slyne Basin, while in the Northern sub basin the~~
746 ~~Upper Triassic Uilleann Halite Member is also present, acting as a second layer of~~
747 ~~mechanical detachment.~~

748 **9.8. Data availability**

749 The data that support the findings of this study were provided by the Petroleum Affairs Division
750 (PAD) and are available for download from [https://www.dccae.gov.ie/en-ie/natural-](https://www.dccae.gov.ie/en-ie/natural-resources/topics/Oil-Gas-Exploration-Production/data/Pages/Data.aspx)
751 [resources/topics/Oil-Gas-Exploration-Production/data/Pages/Data.aspx](https://www.dccae.gov.ie/en-ie/natural-resources/topics/Oil-Gas-Exploration-Production/data/Pages/Data.aspx). Restrictions may
752 apply to the availability of these data, which were used under licence for this study.

753 **10.9. Author contribution**

754 Conor O’Sullivan carried out data analysis, wrote the original text, drafted the figures, and
755 conceptualised the original ideas presented therein. Conrad Childs and Mudasar Saqab
756 provided initial project conceptualisation, supervision and reviewed the final text. John Walsh
757 and Patrick Shannon reviewed the final text.

758 **11.10. Declaration of competing interests**

759 The authors declare that they have no known competing financial interests or personal
760 relationships that could have appeared to influence the work reported in this paper.

761 **12.11. Acknowledgements**

762 This research is funded in part by a research grant from Science Foundation Ireland (SFI)
763 under Grant Number 13/RC/2092 and is co-funded under the European Regional
764 Development Fund, and by the Petroleum Infrastructure Programme (PIP) and its member
765 companies. Efstratios Delogkos is thanked for thoughtful discussions regarding the links
766 between the Slyne Basin and the Bróna and Pádraig basins. Karize Oudit, Neil Jones, Blanca
767 Cantalejo Lopez and Andrew King of CNOOC International are thanked for engaging
768 discussions on the structural evolution of the Slyne Basin. Phil Copestake of Merlin Energy
769 Resources Limited is thanked for providing additional detail on revised biostratigraphic
770 interpretation of the Slyne Basin. The authors would like to thank reviewers Tiago Alves and
771 Amir Joffe for their constructive reviews which greatly improved the manuscript. The authors
772 would like to thank the Petroleum Affairs Division (PAD) of the Department of
773 Communications, Climate Action and Environment (DCCAE), Ireland, for providing access to
774 released well, seismic and potential field datasets. Europa Oil & Gas are thanked for providing
775 access to the Inishkea 2018 reprocessed 3D volume and allowing an arbitrary line from the
776 volume to be shown. Shell Exploration & Production Ireland Ltd. are thanked for providing
777 access to reprocessed volumes of the 1997 Corrib 3D. The authors would also like to thank
778 Schlumberger for providing academic licenses of Petrel to University College Dublin.

779

780 ~~13.12.~~ 12. References

- 781 Ady, B.E. & Whittaker, R.C.: Examining the influence of tectonic inheritance on the evolution
782 of the North Atlantic using a palinspastic deformable plate reconstruction. *Geological*
783 *Society, London, Special Publications*, **470**, 245–264, <https://doi.org/10.1144/SP470.9>.
784 2019.
- 785 Agostini, A., Corti, G., Zeoli, A. & Mulugeta, G.: Evolution, pattern, and partitioning of
786 deformation during oblique continental rifting: Inferences from lithospheric-scale
787 centrifuge models. *Geochemistry, Geophysics, Geosystems*, *10*(11). 2009.
- 788 Alves, T.M., Moita, C., Sandnes, F., Cunha, T., Monteiro, J.H. & Pinheiro, L.M.: Mesozoic-
789 Cenozoic evolution of North Atlantic continental-slope basins: The Peniche basin,
790 western Iberian margin. *AAPG Bulletin*, **90**, 31–60,
791 <https://doi.org/10.1306/08110504138>. 2006.
- 792 Anderson, H., Walsh, J.J. & Cooper, M.R.: The development of a regional-scale intraplate
793 strike-slip fault system; Alpine deformation in the north of Ireland. *Journal of Structural*
794 *Geology*, **116**, 47–63. 2018.
- 795 Badley, M.E.: Late Tertiary faulting, footwall uplift and topography in western Ireland.
796 *Geological Society, London, Special Publications*, **188**, 201–207,
797 <https://doi.org/10.1144/GSL.SP.2001.188.01.11>. 2001.
- 798 Biancotto, F., Hardy, R.J.J., Jones, S.M., Brennan, D. & White, N.J.: Estimating denudation
799 from seismic velocities offshore northwest Ireland. *In: SEG Technical Program*
800 *Expanded Abstracts 2007*. Society of Exploration Geophysicists, 407–411. 2007.
- 801 Bird, P.C., Cartwright, J.A. & Davies, T.L.: Basement reactivation in the development of rift
802 basins: an example of reactivated Caledonide structures in the West Orkney Basin.
803 *Journal of the Geological Society*, **172**, 77–85. 2014.
- 804 Brown, A.R.: Calibrate yourself to your data! A vital first step in seismic interpretation.
805 *Geophysical Prospecting*, **49**, 729–733. 2001.
- 806 Bulois, C., Pubellier, M., Chamot-Rooke, N. & Watremez, L.: From orogenic collapse to
807 rifting: A case study of the northern Porcupine Basin, offshore Ireland. *Journal of*
808 *Structural Geology*, **114**, 139–162, <https://doi.org/10.1016/j.jsg.2018.06.021>. 2018.
- 809 Chapman, T.J., Broks, T.M., Corcoran, D.V., Duncan, L.A. & Dancer, P.N.: The structural
810 evolution of the Erris Trough, offshore northwest Ireland, and implications for
811 hydrocarbon generation. *Petroleum Geology of Northwest Europe: Proceedings of the*
812 *5th Conference*, 455–469. 1999.
- 813 Collanega, L., Siuda, K., Jackson, C. A.-L., Bell, R.E., Coleman, A.J., Lenhart, A., Magee, C.
814 & Breda, A.: Normal fault growth influenced by basement fabrics: The importance of
815 preferential nucleation from pre-existing structures. *Basin Research*, **31**, 659–687,
816 <https://doi.org/10.1111/bre.12327>. 2019.
- 817 Corcoran, D. V & Doré, A.G.: Depressurization of hydrocarbon-bearing reservoirs in
818 exhumed basin settings: evidence from Atlantic margin and borderland basins.

- 819 *Geological Society, London, Special Publications*, **196**, 457–483,
820 <https://doi.org/10.1144/GSL.SP.2002.196.01.25>. 2002.
- 821 Corcoran, D. V & Mecklenburgh, R.: Exhumation of the Corrib Gas Field, Slyne Basin,
822 offshore Ireland. *Petroleum Geoscience*, **11**, 239–256. 2005.
- 823 Corfield, S., Murphy, N. & Parker, S.: The structural and stratigraphic framework of the Irish
824 Rockall Trough. *Petroleum Geology Conference Proceedings*, **5**, 407–420,
825 <https://doi.org/10.1144/0050407>. 1999.
- 826 Corti, G., van Wijk, J., Cloetingh, S. & Morley, C.K.: Tectonic inheritance and continental rift
827 architecture: Numerical and analogue models of the East African Rift system.
828 *Tectonics*, **26**, n/a-n/a, <https://doi.org/10.1029/2006TC002086>. 2007.
- 829 Cunningham, G.A. & Shannon, P.M.: The Erris Ridge: A major geological feature in the NW
830 Irish Offshore Basins. *Journal of the Geological Society*, **154**, 503–508. 1997.
- 831 Dancer, P.N., Algar, S.T. & Wilson, I.R.: Structural evolution of the Slyne Trough. *Petroleum
832 Geology of Northwest Europe: Proceedings of the 5th Conference on the Petroleum
833 Geology of Northwest Europe*, **1**, 445–454. 1999.
- 834 Dancer, P.N. & Pillar, N.W.: Exploring in the Slyne Basin: a geophysical challenge. *The
835 Petroleum Exploration of Ireland's Offshore Basins*, **188**, 209–222. 2001.
- 836 Dancer, P.N., Kenyon-Roberts, S.M., Downey, J.W., Baillie, J.M., Meadows, N.S. & Maguire,
837 K.: The Corrib gas field, offshore west of Ireland. *Geological Society, London,
838 Petroleum Geology Conference series*, **6**, 1035–1046. 2005.
- 839 Doré, A.G., Lundin, E.R., Jensen, L.N., Birkeland, O., Eliassen, P.E. & Fichler, C.: Principal
840 tectonic events in the evolution of the northwest European Atlantic margin. *Petroleum
841 Geology of Northwest Europe: Proceedings of the 5th Conference*, 41–61. 1999.
- 842 Doré, A.G., Lundin, E.R., Fichler, C. & Olesen, O.: Patterns of basement structure and
843 reactivation along the NE Atlantic margin. *Journal of the Geological Society*, **154**, 85–9.
844 2007.
- 845 Droujinine, A., Buckner, S. & Cameron, R.: Full-wave long offset seismic imaging and
846 velocity analysis with gravity and well constraints — a case study from NW Corrib,
847 offshore Ireland. In: *SEG Technical Program Expanded Abstracts 2005*. Society of
848 Exploration Geophysicists, 409–412. 2005.
- 849 Duffy, O.B., Gawthorpe, R.L., Docherty, M. & Brocklehurst, S.H.: Mobile evaporite controls
850 on the structural style and evolution of rift basins: Danish Central Graben, North Sea.
851 *Basin Research*, **25**, 310–330, <https://doi.org/10.1111/bre.12000>. 2013.
- 852 Fazlikhani, H., Fossen, H., Gawthorpe, R.L., Faleide, J.I. & Bell, R.E.: Basement structure
853 and its influence on the structural configuration of the northern North Sea rift. *Tectonics*,
854 **36**, 1151–1177, <https://doi.org/10.1002/2017TC004514>. 2017.
- 855 Fugro.: Field Report Irish Frontier Shallow Coring Project Blocks 19/13 and 27/24 Irish
856 Sector Atlantic Ocean (Volume I). 1994a.

- 857 Fugro.: Field Report Irish Frontier Shallow Coring Project Blocks 19/13 and 27/24 Irish
858 Sector Atlantic Ocean (Volume II). 1994b.
- 859 Gawthorpe, R.L. & Hurst, J.M.: Transfer zones in extensional basins: their structural style
860 and influence on drainage development and stratigraphy. *Journal of the Geological*
861 *Society*, **150**, 1137–1152. 1993.
- 862 Geotrack.: Thermal history reconstruction in well 27/5-1 west of Ireland using apatite fission
863 track analysis and vitrinite reflectance. Report compiled by Gibson, H.J. 1996.
- 864 Geotrack.: Thermal history reconstruction in offshore Ireland well 19/8-1, based on AFTA®
865 and VR data. Report compiled by Green, P.F. 2008.
- 866 Hardy, R.J.J., Querendez, E., Biancotto, F., Jones, S.M., O'Sullivan, J. & White, N.: New
867 methods of improving seismic data to aid understanding of passive margin evolution: a
868 series of case histories from offshore west of Ireland. *Petroleum Geology: From Mature*
869 *Basins to New Frontiers—Proceedings of the 7th Petroleum Geology Conference*, **7**,
870 1005–1012. 2010.
- 871 Henstra, G.A., Rotevatn, A., Gawthorpe, R.L. & Ravnås, R.: Evolution of a major segmented
872 normal fault during multiphase rifting: The origin of plan-view zigzag geometry. *Journal*
873 *of Structural Geology*, **74**, pp.45-63. 2015.
- 874 Henza, A.A., Withjack, M.O. & Schlische, R.W.: How do the properties of a pre-existing
875 normal-fault population influence fault development during a subsequent phase of
876 extension?. *Journal of Structural Geology*, **33**(9), pp.1312-1324. 2011.
- 877 Hudec, M.R. & Jackson, M.P.A.: Terra infirma: Understanding salt tectonics. *Earth-Science*
878 *Reviews*, **82**, 1–28, <https://doi.org/10.1016/j.earscirev.2007.01.001>. 2007.
- 879 Jackson, C.A.L. & Lewis, M.M.: Structural style and evolution of a salt-influenced rift basin
880 margin; the impact of variations in salt composition and the role of polyphase extension.
881 *Basin Research*, **28**, 81–102, <https://doi.org/10.1111/bre.12099>. 2016.
- 882 Jackson, C.A.L., Elliott, G.M., Royce-Rogers, E., Gawthorpe, R.L. & Aas, T.E.: Salt
883 thickness and composition influence rift structural style, northern North Sea, offshore
884 Norway. *Basin Research*, **31**, 514–538, <https://doi.org/10.1111/bre.12332>. 2019.
- 885 Kimbell, G.S., Ritchie, J.D. & Henderson, A.F.: Three-dimensional gravity and magnetic
886 modelling of the Irish sector of the NE Atlantic margin. *Tectonophysics*, **486**, 36–54,
887 <https://doi.org/10.1016/j.tecto.2010.02.007>. 2010.
- 888 Kyne, R., Torremans, K., Güven, J., Doyle, R. & Walsh, J.: 3-D modeling of the Lisheen and
889 silvermines deposits, County Tipperary, Ireland: insights into structural controls on the
890 formation of Irish Zn-Pb deposits. *Economic Geology*, **114**, 93–116,
891 <https://doi.org/10.5382/econgeo.2019.4621>. 2019.
- 892 Lefort, J.P. & Max, M.D.: Development of the Porcupine Seabight: use of magnetic data to
893 show the direct relationship between early oceanic and continental structures. *Journal*
894 *of the Geological Society*, **141**, 663–674, <https://doi.org/10.1144/gsjgs.141.4.0663>.
895 1984.

- 896 McKie, T. & Shannon, P.M.: Comment on 'The Permian-Triassic transition and the onset of
897 Mesozoic sedimentation at the northwestern peri Tethyan domain scale:
898 Palaeogeographic maps and geodynamic implications' by S. Bourquin, A. Bercovici, J.
899 López-Gomez, J. B. Diez, J. Broutin, A. . *Palaeogeography, Palaeoclimatology,*
900 *Palaeoecology*, **311**, 136–143, <https://doi.org/10.1016/j.palaeo.2011.07.016>. 2011.
- 901 Merlin Energy Resources Consortium: The Standard Stratigraphic Nomenclature of Offshore
902 Ireland: An Integrated Lithostratigraphic, Biostratigraphic and Sequence Stratigraphic
903 Framework. Project Atlas. Petroleum Affairs Division, Department of the Environment,
904 Climate and Communications, Special Publication **1/21**. 2020.
- 905 Mohr, P.: Tertiary dolerite intrusions of west-central Ireland. *Proceedings, Royal Irish*
906 *Academy*, **82B**, 53–82. 1982.
- 907 Morley, C.K., Nelson, R. a, Patton, T.L. & Munn, S.G.: Transfer Zones in the East African
908 Rift System and Their Relavance to Hydrocarbon Exploration in Rifts. *American*
909 *Association of Petroleum Geologists Bulletin*, **74, No. 8**, 1234–1253. 1990.
- 910 Morley, C.K., Haranya, C., Phoosongsee, W., Pongwapee, S., Kornsawan, A. & Wonganan,
911 N.: Activation of rift oblique and rift parallel pre-existing fabrics during extension and
912 their effect on deformation style: examples from the rifts of Thailand. *Journal of*
913 *Structural Geology*, **26**, 1803–1829. 2004.
- 914 Musgrove, F.W. & Mitchener, B.: Analysis of the pre-tertiary rifting history of the Rockall
915 Trough. *Petroleum Geoscience*, **2**, 353–360, <https://doi.org/10.1144/petgeo.2.4.353>.
916 1996.
- 917 Naylor, D., Shannon, P. & Murphy, N.: *Irish Rockall Basin Region - a standard structural*
918 *nomenclature system*. Petroleum Affairs Division, Special Publication 1/99. 1999.
- 919 Naylor, D. & Shannon, P.M.: The structural framework of the Irish Atlantic Margin. *Geological*
920 *Society, London, Petroleum Geology Conference series*, **6**, 1009–1021,
921 <https://doi.org/10.1144/0061009>. 2005.
- 922 O'Sullivan, C. & Childs, C.: Kinematic interaction between stratigraphically discrete salt
923 layers; the structural evolution of the Corrib gas field, offshore NW Ireland. *Marine and*
924 *Petroleum Geology*, **133**, 105274, <https://doi.org/10.1016/j.marpetgeo.2021.105274>.
925 2021.
- 926 O'Sullivan, C.M., Childs, C.J., Saqab, M.M., Walsh, J.J. & Shannon, P.M.: The influence of
927 multiple salt layers on rift-basin development; The Slyne and Erris basins, offshore NW
928 Ireland. *Basin Research*, 1–31, <https://doi.org/10.1111/bre.12546>. 2021.
- 929 Osagiede, E.E., Rotevatn, A., Gawthorpe, R., Kristensen, T.B., Jackson, C.A.L. & Marsh, N.:
930 Pre-existing intra-basement shear zones influence growth and geometry of non-colinear
931 normal faults, western Utsira High–Heimdal Terrace, North Sea. *Journal of Structural*
932 *Geology*, **130**, 103908, <https://doi.org/10.1016/j.jsg.2019.103908>. 2020.
- 933 Pereira, R. & Alves, T.M.: Margin segmentation prior to continental break-up: A seismic-
934 stratigraphic record of multiphased rifting in the North Atlantic (Southwest Iberia).
935 *Tectonophysics*, **505**, 17–34, <https://doi.org/10.1016/j.tecto.2011.03.011>. 2011.

- 936 [Pereira, R. & Alves, T.M.: Crustal deformation and submarine canyon incision in a Meso-](#)
 937 [Cenozoic first-order transfer zone \(SW Iberia, North Atlantic Ocean\). *Tectonophysics*,](#)
 938 [601, 148–162. <https://doi.org/10.1016/j.tecto.2013.05.007>. 2013](#)
- 939 [Pereira, R., Alves, T.M. & Mata, J.: Alternating crustal architecture in West Iberia: A review](#)
 940 [of its significance in the context of NE Atlantic rifting. *Journal of the Geological Society*,](#)
 941 [174, 522–540. <https://doi.org/10.1144/jgs2016-050>. 2017.](#)
- 942 Philippon, M. & Corti, G.: Obliquity along plate boundaries. *Tectonophysics*, 693, pp.171-
 943 182. 2016.
- 944 Phillips Petroleum Company: Phillips Petroleum Company Ireland 26/30-1 Final Well Report.
 945 1982.
- 946 Phillips, T.B., Jackson, C.A., Bell, R.E. & Duffy, O.B.: Oblique reactivation of lithosphere-
 947 scale lineaments controls rift physiography – the upper-crustal expression of the
 948 Sorgenfrei–Tornquist Zone, offshore southern Norway. *Solid Earth*, 9, 403–429. 2018.
- 949 Phillips, T.B., Fazlikhani, H., Gawthorpe, R.L., Fossen, H., Jackson, C.A.L., Bell, R.E.,
 950 Faleide, J.I. & Rotevatn, A.: The Influence of Structural Inheritance and Multiphase
 951 Extension on Rift Development, the Northern North Sea. *Tectonics*, 38, 4099–4126,
 952 <https://doi.org/10.1029/2019TC005756>. 2019.
- 953 Robeson, D., Burnett, R.D. & Clayton, G.: The Upper Palaeozoic Geology of the Porcupine,
 954 Erris and Donegal Basins, Offshore Ireland. *Irish Journal of Earth Sciences*, 9, 153–
 955 175. 1988.
- 956 Rodríguez-Salgado, P., Childs, C., Shannon, P.M. & Walsh, J.J.: Structural evolution and the
 957 partitioning of deformation during basin growth and inversion: A case study from the
 958 Mizen Basin Celtic Sea, offshore Ireland. *Basin Research*, 1–24,
 959 <https://doi.org/10.1111/bre.12402>. 2019.
- 960 Rohrman, M.: Prospectivity of volcanic basins: Trap delineation and acreage de-risking.
 961 *AAPG Bulletin*, 91, 915–939. 2007.
- 962 Saqab, M.M., Childs, C., Walsh, J. & Delogkos, E.: Multiphase deformation history of the
 963 Porcupine Basin, offshore west Ireland. *Basin Research*, 1–22,
 964 <https://doi.org/10.1111/bre.12535>. 2020.
- 965 Schiffer, C., Doré, A.G., Foulger, G.R., Franke, D., Geoffroy, L., Gernigon, L., Holdsworth,
 966 R.E., Kuszniir, N., Lundin, E., McCaffrey, K., Peace, A.L., Petersen, K.D., Phillips, T.B.,
 967 Stephenson, R., Stoker, M.S. & Welford J.K.: Structural inheritance in the North
 968 Atlantic. *Earth-Science Reviews*, 102975.
 969 <https://doi.org/10.1016/j.earscirev.2019.102975>. 2019.
- 970 Schlische, R.W., Withjack, M.O. & Eisenstadt, G.: An experimental study of the secondary
 971 deformation produced by oblique-slip normal faulting. *AAPG bulletin*, 86(5), pp.885-906.
 972 2002.
- 973 Schumacher, M.E.: Upper Rhine Graben: Role of preexisting structures during rift evolution.
 974 *Tectonics*, 21. 2002.

Formatted: Font: Arial, 11 pt

- 975 Scotchman, I.C. & Thomas, J.R.W.: Maturity and hydrocarbon generation in the Slyne
976 Trough, northwest Ireland. *The Petroleum Geology of Ireland's Offshore Basins*, **93**,
977 385–412. 1995.
- 978 Shannon, P.M.: The development of Irish offshore sedimentary basins. *Journal of the
979 Geological Society*, **148**, 181–189. 1991.
- 980 Shannon, P.M.: Old challenges, new developments and new plays in Irish offshore
981 exploration. *Geological Society, London, Petroleum Geology Conference series*, **8**,
982 171–185, <https://doi.org/10.1144/PGC8.12>. 2018.
- 983 Stein, A.M.: Basement controls upon basin development in the Caledonian foreland, NW
984 Scotland. *Basin Research*, **1**, 107–119, [https://doi.org/10.1111/j.1365-
985 2117.1988.tb00008.x](https://doi.org/10.1111/j.1365-2117.1988.tb00008.x). 1988.
- 986 Štolfová, K. & Shannon, P.M.: Permo-Triassic development from Ireland to Norway: basin
987 architecture and regional controls. *Geological Journal*, **44**, 652–676. 2009.
- 988 Tate, M.P.: The Clare Lineament: A relic transform fault west of Ireland. *Geological Society
989 Special Publication*, **62**, 375–384, <https://doi.org/10.1144/GSL.SP.1992.062.01.28>.
990 1992.
- 991 Tate, M.P. & Dobson, M.R.: Late Permian to early Mesozoic rifting and sedimentation
992 offshore NW Ireland. *Marine and Petroleum Geology*, **6**, 49–59,
993 [https://doi.org/10.1016/0264-8172\(89\)90075-5](https://doi.org/10.1016/0264-8172(89)90075-5). 1989.
- 994 Tommasi, A. & Vauchez, A.: Continental rifting parallel to ancient collisional belts: An effect
995 of the mechanical anisotropy of the lithospheric mantle. *Earth and Planetary Science
996 Letters*, **185**, 199–210, [https://doi.org/10.1016/S0012-821X\(00\)00350-2](https://doi.org/10.1016/S0012-821X(00)00350-2). 2001.
- 997 Trueblood, S. & Morton, N.: Comparative Sequence Stratigraphy and Structural Styles of the
998 Slyne Trough and Hebrides Basin. *Journal of the Geological Society*, **148**, 197–201.
999 1991.
- 1000 Underhill, J.R. & Partington, M.A.: Jurassic thermal doming and deflation in the North Sea:
1001 Implications of the sequence stratigraphic evidence. *Petroleum Geology Conference
1002 Proceedings*, **4**, 337–345, <https://doi.org/10.1144/0040337>. 1993.
- 1003 Van Hoorn, B.: The south Celtic Sea/Bristol Channel Basin: origin, deformation and inversion
1004 history. *Tectonophysics*, **137**, [https://doi.org/10.1016/0040-1951\(87\)90325-8](https://doi.org/10.1016/0040-1951(87)90325-8). 1987.
- 1005 Vendeville, B.C. & Jackson, M.P.A.: The fall of diapirs during thin-skinned extension. *Marine
1006 and Petroleum Geology*, **9**, 354–371, [https://doi.org/10.1016/0264-8172\(92\)90048-J](https://doi.org/10.1016/0264-8172(92)90048-J).
1007 1992.
- 1008 Walsh, A., Knag, G., Morris, M., Quinquis, H., Tricker, P., Bird, C. & Bower, S.: Petroleum
1009 geology of the Irish Rockall Trough – a frontier challenge. *Petroleum Geology of
1010 Northwest Europe: Proceedings of the 5th Conference*, 433–444. 1999.
- 1011 Walsh, J.J. & Watterson, J.: Geometric and kinematic coherence and scale effects in normal
1012 fault systems. *Geological Society Special Publication*, **56**, 193–203,
1013 <https://doi.org/10.1144/GSL.SP.1991.056.01.13>. 1991.

- 1014 Wilson, R.W., Holdsworth, R.E., Wild, L.E., Mccaffrey, K.J.W., England, R.W., Imber, J. &
1015 Strachan, R.A.: Basement-influenced rifting and basin development: A reappraisal of
1016 post-Caledonian faulting patterns from the North Coast Transfer Zone, Scotland.
1017 *Geological Society Special Publication*, **335**, 795–826,
1018 <https://doi.org/10.1144/SP335.32>. 2010.
- 1019 Worthington, R.P. & Walsh, J.J.: Structure of Lower Carboniferous basins of NW Ireland,
1020 and its implications for structural inheritance and Cenozoic faulting. *Journal of*
1021 *Structural Geology*, **33**, 1285–1299. 2011.
- 1022 Ziegler, P.A. & Dèzes, P.: Crustal evolution of Western and Central Europe. *Geological*
1023 *Society, London, Memoirs*, **32**, 43–56. 2006.